Testing of the C1 Coil

October 20, 2006

NCSX-TEST-14-01-00

Prepared by: _____

Wayne Reiersen

Reviewed by: _____

Geoff Gettelfinger

Reviewed by: _____

Kevin Freudenberg

Reviewed by: _____

David Williamson

Reviewed by: _____

Art Brooks

Approved by: _____

Brad Nelson

Table of Contents

Table of Tables

Table of Figures

1   EXECUTIVE SUMMARY

The C1 coil was cold tested in June 2006. Prior to cooling down to cryogenic temperature, a megger test was performed. The insulation resistance to ground dropped markedly at 7kV. The coil was re-tested with a 9V Digital Voltmeter (DVM) and showed a resistance to ground of only 2Mohms. The coil had previously been tested following vacuum pressure impregnation (VPI) at 7.5kV and registered a resistance to ground of 75Gohms. The weak link in the insulation was traced to the lead block area. It was decided the resistance to ground was adequate to proceed with cold testing. The coil was cooled down to cryogenic temperature. The resistance to ground was re-measured using the DVM and improved modestly to above 4Mohms. The coil was then tested at full current without incident.

Following the test, the lead block area was opened. In the process of opening the lead block area, the upper chill plate was partially separated from the winding pack. The resistance to ground was checked and measured 15Gohms at 7.5kV, a dramatic improvement. It was determined that the upper chill plate was the likely culprit and represented a weak link in the design. The decision was made to remove the upper chill plate on C1 and all coils in process (C3 and beyond). No significant impact on coil performance was identified. With the chill plate removed, the resistance to ground was checked at 5kV and measured 110Gohms, which exceeds our requirements. Additional insulation was applied in this area and the repair procedure was completed.

The C2 coil was manufactured the same way as the C1 coil and showed a resistance to ground of 22Gohms at 7.5kV following VPI. The suspect chill plate on the C3 coil was removed prior to VPI. Testing of the C3 coil following VPI showed a much healthier resistance to ground of 150Gohms at 7.5kV, which is comparable to C1 after repair and much higher than C2. This trend continued for C4 which had a 150Gohm resistance at 7.5kV. The project now plans to make the same repair to C2 that was made to C1 because of the improved resistance to ground demonstrated on the C1, C3 and C4 coils.

The coil resistance, the observed temperature rise, and the cooldown rate between shots were all in agreement with predicted values during the testing of the C1 coil. The coil resistance was measured to be 1.7 milli-ohms at 89K. The observed temperature rise was 28K. The characteristic temperature decay time between shots was measured to be 13 minutes. These results validated our electrical and thermal models of the coil, providing high confidence that the coil will behave thermally and electrically during operation as predicted.

Displacements across the width of the coil (approximately 2m) during a pulse were measured with a displacement gauge and were in excellent agreement (within 2%) with predicted values. The displacement measurements are very significant because they are a measure of the response of the whole coil assembly, not just a local area, and provide high confidence that the structural modeling of the coil assembly is reasonable.

In addition to the displacement measurements, conventional (resistive) strain gauges were applied to the winding form and winding pack prior to cold testing. These gauges were used because of previous favorable experience on ATF. Bench tests were conducted prior to testing C1 that confirmed that these gauges could be used in a cryogenic environment. However, the test data from these gauges during testing of the C1 coil was not usable. Examination of the test data revealed that the substantial voltage ripple in the power supply and magneto-resistive effects in the strain gauges precluded getting useful data. Failure to get good strain gauge data from the C1 test limited validation of the structural model of a single coil to the displacement measurement results and left us without a qualified system for monitoring the structural behavior of the modular coils during experimental operations.

The Project plans to substitute fiber optic strain gauges for the non-functional resistive gauges on the production coils. The fiber optic gauges are immune to voltage ripple and magneto-resistive effects. Such gauges have been used very successfully on the NSTX TF coils, albeit at room temperature. They are being qualified for use at cryogenic temperatures at ORNL. The gauges will begin being installed on the production coils once the qualification testing at ORNL is successfully concluded.

2   TEST SETUP

2.1   Instrumentation

2.1.1   Thermocouples

Eighteen Type E thermocouples were installed in the test setup. The data acquisition system provided six channels for thermocouple data. The locations for the thermocouples are listed in Table 5-1. Two thermocouples (TC2 and TC3) were embedded in deep holes in the winding form. One thermocouple was installed on the exterior of the winding pack (TC17). One thermocouple was installed on an inboard supply coolant tube (TC7) and another on an outboard return coolant tube (TC9). Thermocouples were typically insulated with bat insulation from the cryostat environment to avoid convective cooling of the thermocouple directly. The final channel monitored the temperature inside the cryostat near the midplane elevation (TC18).

2.1.2   Strain Gages

Fifteen strain gages were installed. The strain gages were manufactured by Vishay (H06A-AC1-125-700). The data acquisition system provided fourteen operable channels for the strain gage data. The locations for the strain gages are listed in Table 5-2. Of the fourteen operable channels, ten channels monitored strain gages mounted on the winding form. Nine of these strain gages were mounted at the base of the tee. The tenth was mounted on the exterior surface of the winding form near where the leads penetrate the winding form. The active strain gages mounted on the winding form were paired with dummy strain gages mounted approximately 1 inch off the winding form on a stainless steel substrate connected to the casting with a stud. Strain gages were typically insulated with bat insulation to avoid introducing temperature differences between the active and dummy gages due to convective cooling. Some strain gages, e.g., SG15, had a copper sleeve around the stud for improved thermal contact. The intent of the dummy gages was to remove the thermal output so the apparent strain reflected the true mechanical strain. Photographs of strain gage installations (without thermal insulation) are provided in Figure 5-34 through Figure 5-39.

The remaining four strain gages were installed on the exterior of the winding pack. There was no substrate to mount dummy gages so the dummy gage was actually installed on the winding pack on the opposite side of the tee. This was intended to remove the thermal output from cooldown to cryogenic temperature. However, the apparent strain due to EM loading during a pulse would be the difference between these two active gages. Strain gages mounted on the winding pack are apparent in Figure 5-34.

The strain gages mounted at the base of the tee and on the winding pack were oriented either in the direction of the winding pack or normal (transverse) to the direction of the winding pack. Typically, two strain gages, one in the direction of the winding pack and one in the transverse direction were installed at each of the clamp locations selected as shown in Figure 5-36.

2.1.3   Deflection Monitor

A deflection monitor was mounted on the flanges to measure the linear deflection across the bore of the coil during a pulse. The gage and digital readout were located outside the cryostat. The readings on the digital readout were recorded with a video camera. Measurements of interest were the maximum change in deflection during a pulse and the change in deflection before and after a pulse.

3   TEST RESULTS

3.1   Electrical Testing Prior to Cooldown

The C1 coil was cold tested in June 2006. Prior to cooling down to cryogenic temperature, a megger test was performed. The insulation resistance to ground dropped markedly at 7kV. The coil was re-tested with a 9V Digital Voltmeter (DVM) and showed a resistance to ground of only 2Mohms. The coil had previously been tested following vacuum pressure impregnation (VPI) at 7.5kV and registered a resistance

to ground of 75Gohms. The weak link in the insulation was traced to the lead block area. It was decided the resistance to ground was adequate to proceed with cold testing. The coil was cooled down to cryogenic temperature. The resistance to ground was re-measured using the DVM and improved modestly to above 4Mohms. The coil was then tested at full current without incident.

Following the test, the lead block area was opened. In the process of opening the lead block area, the upper chill plate was partially separated from the winding pack. The resistance to ground was checked and measured 15Gohms at 7.5kV, a dramatic improvement. It was determined that the upper chill plate was the likely culprit and represented a weak link in the design. The decision was made to remove the upper chill plate on C1 and all coils in process (C3 and beyond). No significant impact on coil performance was identified. With the chill plate removed, the resistance to ground was checked at 5kV and measured 110Gohms, which exceeds our requirements. Additional insulation was applied in this area and the repair procedure was completed.

The C2 coil was manufactured the same way as the C1 coil and showed a resistance to ground of 22Gohms at 7.5kV following VPI. The suspect chill plate on the C3 coil was removed prior to VPI. Testing of the C3 coil following VPI showed a much healthier resistance to ground of 150Gohms at 7.5kV, which is comparable to C1 after repair and much higher than C2. This trend continued for C4 which had a 150Gohm resistance at 7.5kV. The project now plans to make the same repair to C2 that was made to C1 because of the improved resistance to ground demonstrated on the C1, C3 and C4 coils.

3.2   Cooldown

Cooldown of the C1 coil began on June 11 and continued until shots began to be taken on June 15. Cooldown was initiated by introducing product from the LN2 supply line. The line is used intermittently so initially, the product was warm gas. A maximum temperature difference of 50K was administratively enforced during cooldown. As the line cooled, so did the gas being supplied until eventually it became 2-phase product and then mostly liquid. The liquid was caught in a tank in the center of the cryostat. The tank measured 12" on each side. The liquid column was approximately 34" tall.

During the first 40 hours, the cooldown followed an exponential curve that featured a decay time of 18 hours with an asymptote of approximately 120K. The cooldown versus time for one of the thermocouples embedded in the winding form is shown in Figure 3-1.
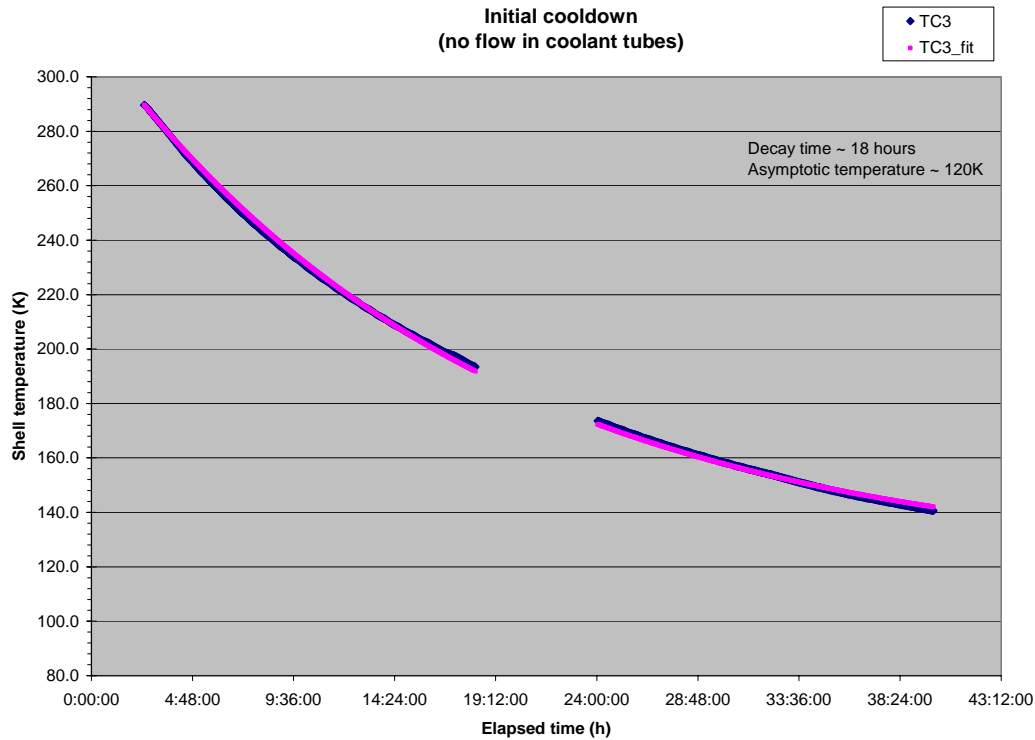
Figure 3-1 Winding form cooldown versus time

The SRD requirement is for the modular coils to be cooled down to operating temperature (nominally 80K) within 96 hours. Cooling from 293K to 90K assuming an 85K interior temperature would require a decay time of 25 hours (if an exponential model applied). The cooldown of C1 was based on cooling the interior and exterior of the shell. In the stellarator, the space between the modular coil and vacuum vessel (the interior of the shell) will be filled with insulation. Therefore, the surface area exposed to GN2 will be reduced by more than half. The decay time should be inversely proportional to the exposed surface area and the convective heat transfer coefficient. The decrease in surface area will have to be compensated by an increase in the convective heat transfer coefficient. This may require a change from natural (free) convection to forced convection.

The asymptotic (bath) temperature of the cryostat was well above the desired 80K. This too needs to be addressed in the cryostat cooling system design. In equilibrium, the cryostat system can be modeled as shown in Figure 3-2.

$$Q_{out} = Q_{cryo} + Q_{in} = \dot{m} \times h_g$$

$T_{amb} = 293K$ $T_{cryo} \sim 120K$ (avg)

$Q_{in} = \dot{m} \times h_f$

Q_{cryo}

$T_{tank} \sim 80K$

Figure 3-2 Cryostat heat balance

Assuming a surface area of 32 m2 for the cryostat and a 6-inch wall of panels with an insulating value of R6 per inch, the heat leak into the cryostat would be approximately 860 W. If the temperature of the exhaust gas is 120K (the asymptotic temperature calculated for initial cooldown), then a mass flow of 0.0036 kg/s is required. Two thirds of the heat is removed by evaporating LN2 with the balance removed by the temperature rise in the exhaust gas. In the stellarator, we want to minimize any temperature rise in the exhaust gas in order to keep the temperature as close to 80K as possible.

When the average temperature inside the cryostat approached 130K, 2-phase product was introduced into the coolant channels. Ultimately, single phase LN2 was circulated through the 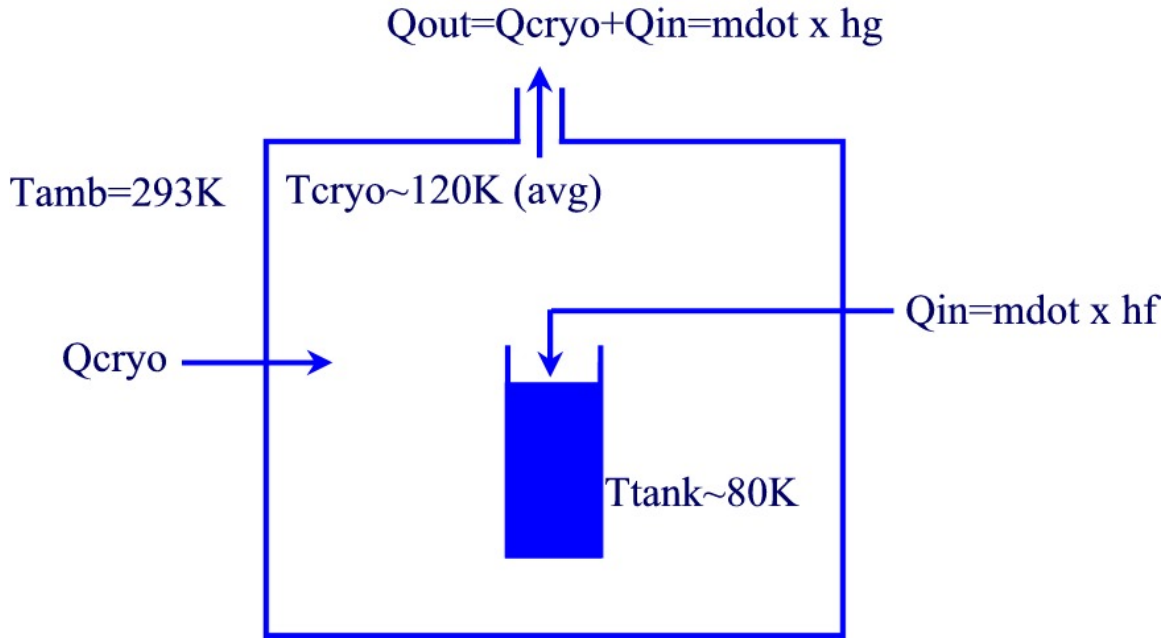winding pack which brought the average chamber temperature to 100K (TC18 in Figure 3-3) in approximately ten (10) hours. This temperature was well above the 80K temperature envisioned for the coil environment. Thermocouples embedded in the winding form near the winding pack read as low as 92K (TC3) and 94K (TC2). The inlet temperature read as low as 83K (TC7) with an outlet temperature of 87K (TC9). Note that the beneficial effect of cooling the chamber brought about by cooling the winding pack with LN2 will not be manifest (at least not directly) in the stellarator because the winding pack will be thermally insulated. Note also that there were no measurements of the winding form temperature apart from the two thermocouples embedded deep in the winding form close to the winding pack. Additional thermocouples should be provided on the winding forms in the stellarator so temperature differences can be monitored.

The flow rate of LN2 was not measured during the testing of the C1 coil. However, it can be estimated by considering the pump characteristics. A pump performance curve is provided in Figure 5-4. With the pump connected to the C1 coil, a pressure drop of 24 psid was measured with the pump operating at 5800 rpm suggesting a flow rate of 8.3 gpm. During actual C1 testing, the pump operated at 4800 rpm with a measured pressure drop of 16.5 psid and an estimated flow rate of 6.5 gpm.

The temperature of the winding form in the wings was not monitored. In the stellarator, this is an area of concern. The plasma-side surface of the wings is thermally insulated. The outside surface faces, but is not in good thermal contact with the plasma-side surface of the winding form into which it nests. It may be beneficial, perhaps necessary, to circulate gaseous nitrogen through the coolant tubes in order to cool the wings and also expedite initial cooldown.
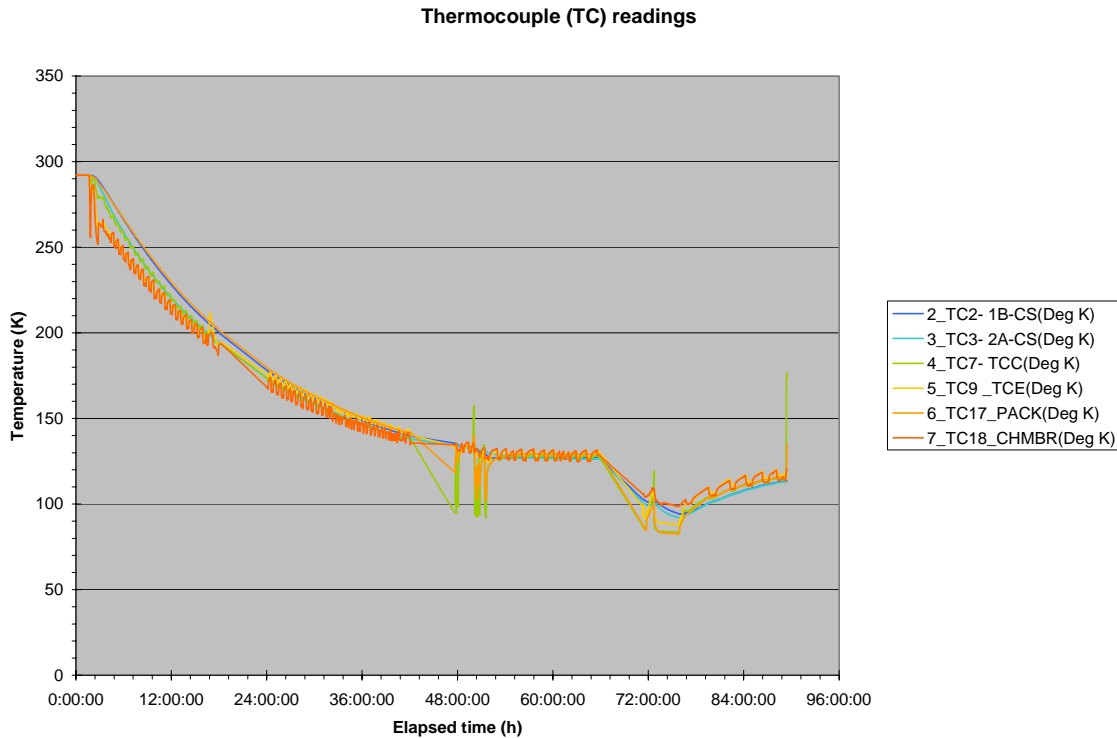
Thermocouple (TC) readings

Figure 3-3 Thermocouple readings during initial cooldown

The discussion thus far has focused on the average cryostat temperature. Actually this is the temperature measured by a thermocouple (TC18) mounted approximately one inch off the interior surface of the cryostat and 24 inches off the floor of the cryostat (with an interior height of 48 inches). As the gas pressure inside the cryostat was only slightly above atmospheric pressure, the gas evolving from the open-top tank was certainly near 78K which is significantly lower than the chamber temperature measured by the thermocouple. This difference is reminiscent of the temperature differentials observed inside the cryostat for the LN2 delivery system. Constructed in a manner similar to the coil cryostat, this cryostat has an interior height of 68 inches with an open-top LN2 tank. There are three thermocouples mounted inside. One is 8 inches off the floor of the cryostat. The second is 34 inches off the floor of the cryostat. The third is 65 inches off the floor of the cryostat. The temperature of the nitrogen gas in this cryostat is highly stratified. Temperature differences between the upper and lower thermocouples of 68K (from 80K on the bottom to 148K on the top) have been observed. This observation along with the measured midplane temperature in the neighborhood of 120K during C1 testing underscores the need for circulating nitrogen gas within the cryostat for effective cooling.

3.3   Coil Testing

A series of shots were taken with the coil cold on June 15 and June 16. Coil currents were increased from 5kA to 36.5kA. Coil currents were then decreased down to 15kA. The prescribed waveform was the same for all of the test shots. There was a 1s linear rise to full current, a 0.2s flattop, and a 1s linear ramp down to zero current. Intermediate 2kA shots were taken at approximately 10 minute intervals to measure the coil resistance and infer the average winding temperature. Test shots (above 2kA) were not initiated unless the coil resistance measured in the 2kA shots was at or below 1.8 milli-ohms which corresponds to an average winding temperature of approximately 98K. The coil was then allowed to warm back to room temperature during which time additional 15kA shots were taken. The sequence is shown in Table 3-1.

2kA shots and shots in which there were trips are not shown. All test data is available from the following URL:

http://ncsx.pppl.gov/NCSX_Engineering/R&D_Results/PPPL/C1%20Testing/Index_C1%20testing.htm

The purpose of the test shots is to validate our modeling of coil performance. If we successfully predict the performance of the C1 coil in the test shots, then we have increased confidence in the predicted performance during stellarator operation. There are several aspects of coil performance to be modeled, including cooldown between shots and incremental stresses and displacements due to EM and thermal loads during a shot.

Table 3-1 Summary of test shots

Shot number	Date and time	Max current (kA)	Pre-shot outlet (TC9) temperature (K)
121400	6/15 2:54:31pm	5	87.2
121405	6/15 3:33:43pm	15	87.6
121408	6/15 3:52:39pm	25	87.6
121419	6/16 9:54:18am	35	92.1
121439	6/16 12:06:43pm	36.5	89.6
121453	6/16 1:27:56pm	36.5	88.9
121461	6/16 2:31:55pm	36.5	88.8
121468	6/16 3:33:33pm	25	88.6
121471	6/16 3:59:03pm	15	88.6
121537	6/23 9:29:30am	15	256.0
121540	6/23 10:14:37am	15	258.2

3.3.1   Cooldown between Shots

There are two diagnostics from which we can monitor cooldown between shots. The first diagnostic is the thermocouple data. There was a thermocouple mounted on the outside of the winding pack near hole 85 (TC17). The second diagnostic is the temperature inferred from the 2kA shots run between test shots.

Consider cooldown following Shot 121461 which was a full current (36.5kA) shot. A plot is shown in Figure 3-4. The thermocouple mounted on the surface of the winding pack (TC17) starts off with a temperature reading of 83.2K which is approximately equal to the inlet temperature reading 83.8K (TC7). During a shot, the temperature of the winding pack is estimated to increase by approximately 28K within the 2.2s shot duration. The temperature of the chill plate under TC17 rises over the next 4 minutes by 5.3K. Thereafter, the temperature of the chill plates drops with a decay time of approximately 13 minutes. After 15 minutes, TC17 still reads 85.7K which is 2.5K higher than the initial temperature. In order to accommodate the soak time to establish the temperature gradients needed to conduct the heat to the coolant and the subsequent thermal decay time, it appears necessary to accept a pre-shot winding pack temperature which is significantly higher than the coolant temperature.

There are two phenomena that are occurring – temperature redistribution and cooling. The temperature on the surface of the winding pack can be approximated with a simple model per Equation 3-1.

Equation 3-1

$$T = T_a + (T_0 - T_a + \Delta T(1 - e^{-\alpha t}))e^{-\beta t}.$$

T_a is the asymptotic temperature to which the winding pack surface would decay and should approximate the local coolant temperature. T_0 is the initial temperature. ΔT is the increase in the surface temperature in the absence of cooling following a shot. α is the characteristic temperature redistribution rate. β is the characteristic heat removal rate. With an assumed coolant temperature of 83K (slightly less than the initial temperature of 83.2K), the "best fit" parameters are a ΔT of 9K, a characteristic temperature redistribution time ($1/\alpha$) of 2 minutes, and a characteristic cooling time ($1/\beta$) of 13 minutes. Although the adiabatic temperature rise in the copper conductor is calculated to be 28K, the winding form in the vicinity of the winding pack acts as a heat sink as evidenced by the rise in temperatures in winding form thermocouples (TC2 and TC3). The assumed coolant temperature of 83K is reasonable because more than one hour transpired since the previous full current pulse. The agreement between the cooldown data following Shot 121461 and the simple model with these parameters is good as shown in Figure 3-5.
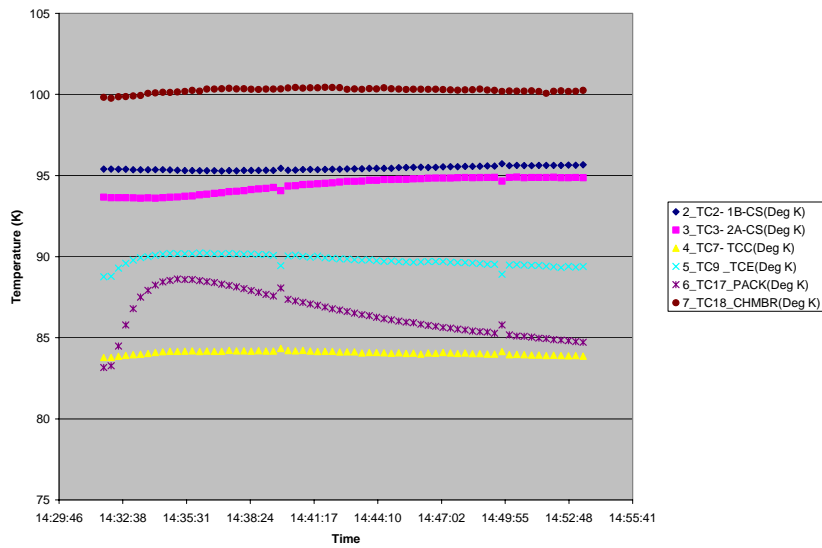

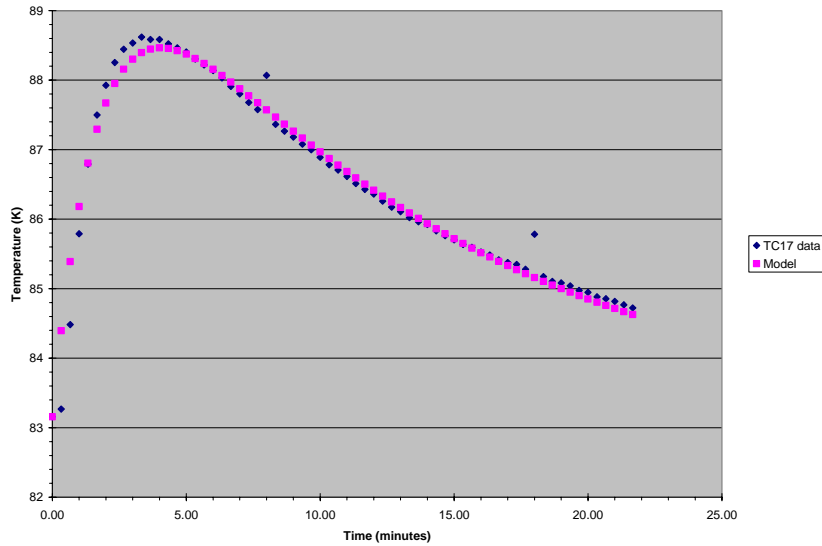**Figure 3-4 Cooldown following Shot 121461**

12

Figure 3-5 Winding surface temperature following Shot 121461

An ANSYS model of the winding pack was generated to model cooldown between pulses. The ANSYS model did not include the epoxy shell (of unknown thickness) outside the chill plates to which the thermocouple was attached. However, it is instructive to compare the thermal decay rate measured at thermocouple and predicted for the chill plates in the vicinity of the thermocouple. The cooldown between pulses of the chill plates is shown in Figure 3-6 for four points in time.
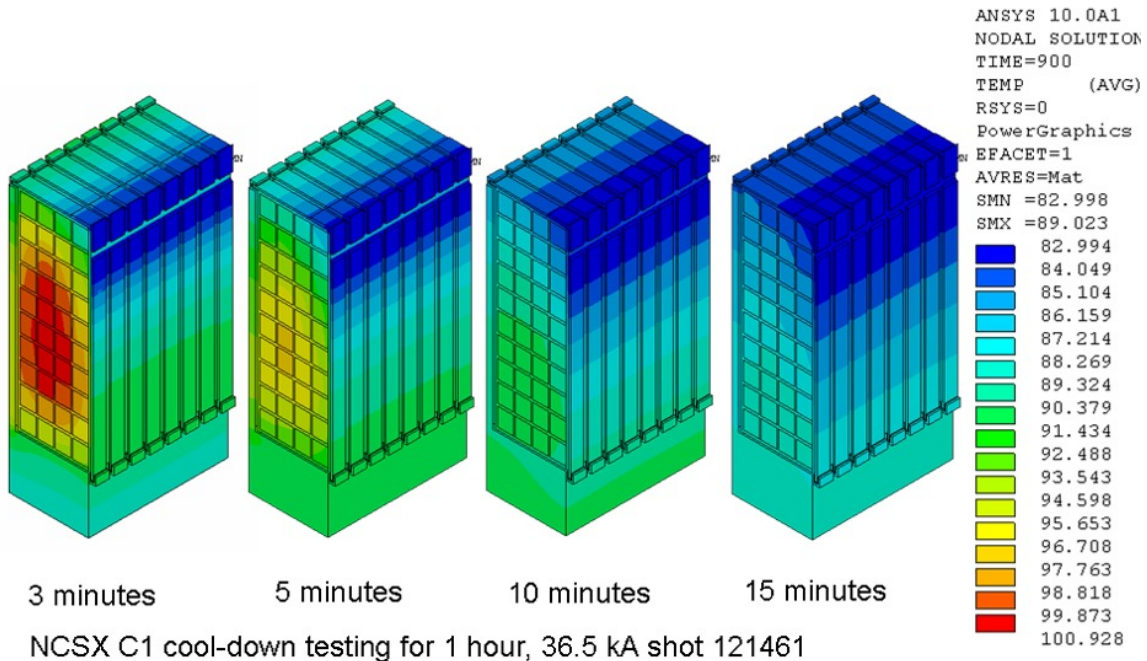

Figure 3-6 ANSYS modeling of cooldown following Shot 121461

Thermal decay rates along the height of the chill plate were calculated and matched well with the thermal decay rate observed for the thermocouple (TC17) mounted on the epoxy just outside the chill plate, closer

to the coolant tubes than the base of the tee[1]. A comparison of the measured and calculated thermal decay rates (β in Equation 3-1) are shown in Figure 3-7.
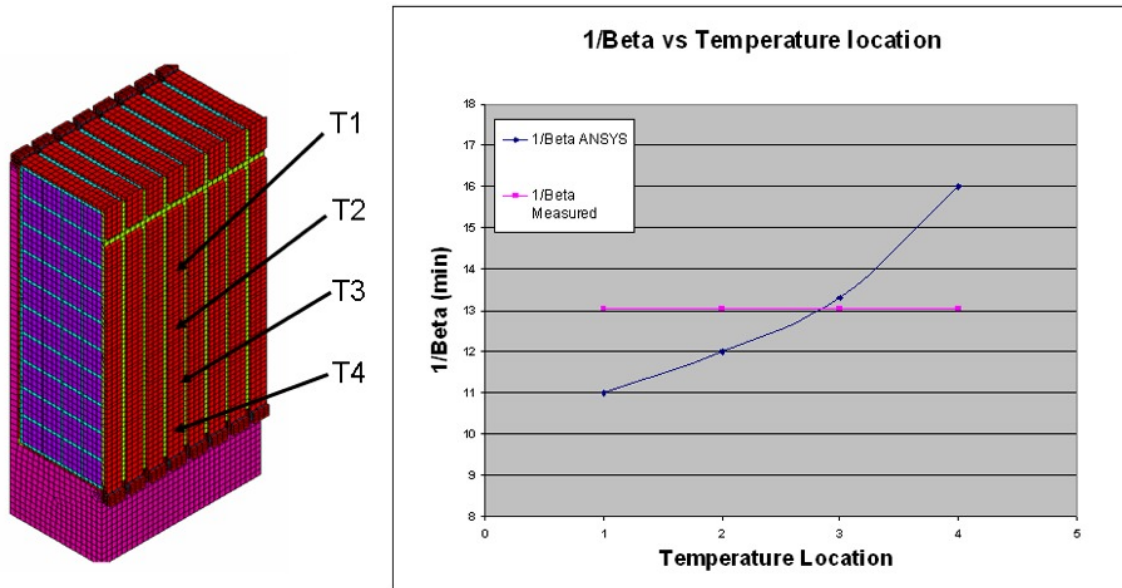
Figure 3-7 Comparison of measured and calculated thermal decay rates

The second diagnostic is the average winding temperature inferred from the 2kA shots between test shots. The data is shown in Figure 3-8. Clearly, there is significant noise in the measurement and variation during a shot due to current redistribution among the four parallel conductors (even at constant net current). Shot 121462 was run at 2:40pm (8 minutes after Shot 121461) and registered a resistance in the range of 1.8-2.3 milli-ohms (2.05 milli-ohm median). Shot 121463 was run at 2:50pm (18 minutes after Shot 121461) and registered a resistance in the range of 1.5-2.0 milli-ohms (1.75 milli-ohm median).   The median temperatures during Shots 121462 and 121463 are calculated to correspond to temperatures of 103.7K and 96.5K respectively.

---

[1] G. Gettelfinger, private communication

Figure 3-8 Winding resistance measurements

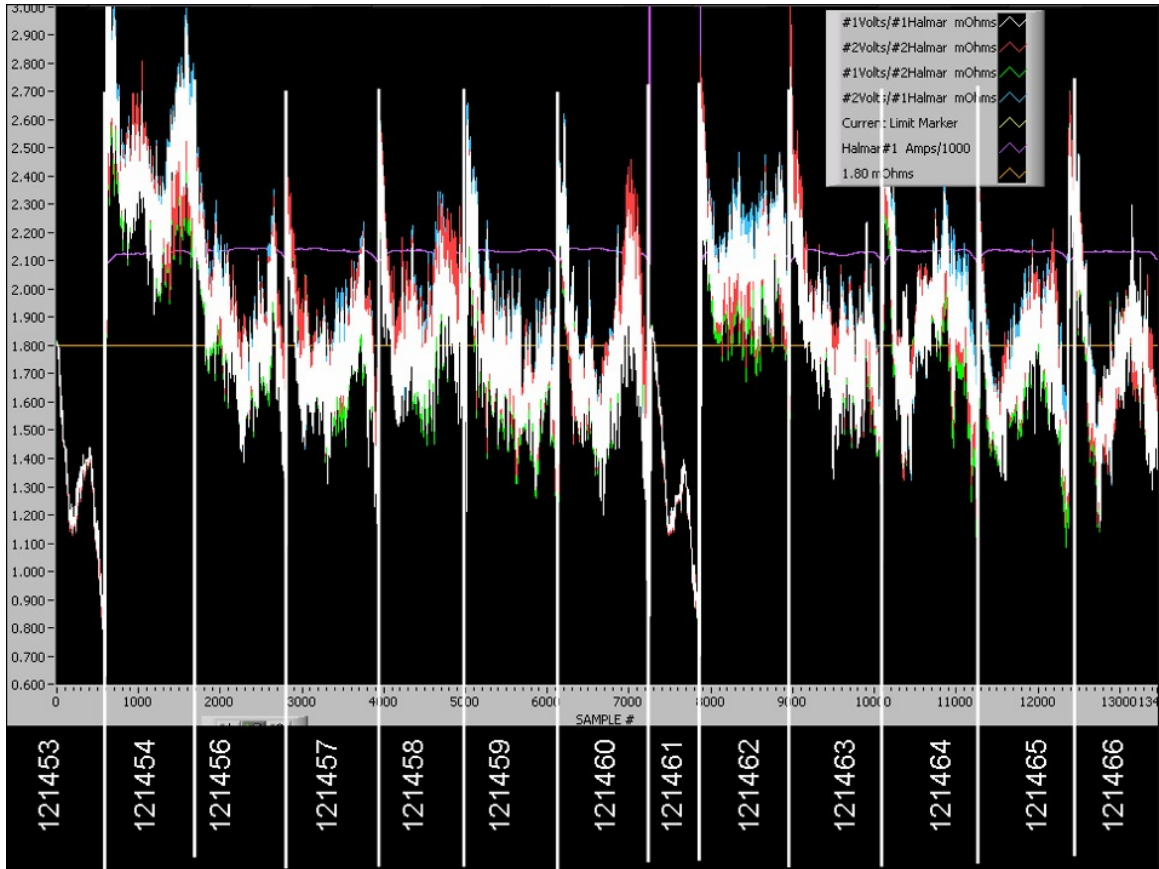The coil resistance was measured manually (outside the cryostat) at 12:30pm prior to any shots. This measurement has none of the ripple associated with the 2kA shots. The resistance was measured to be 1.7 milli-ohms which corresponds to an average winding temperature of 89K. The outlet temperature of the coolant was also measured to be 89K at this time. If we assume that the asymptotic temperature of the winding pack (T_a) is 89K and the decay time is 13 minutes (as calculated for the winding pack surface), then the temperature rise during Shot 121461 (ΔT) is estimated to be 28K assuming the simple exponential model in Equation 3-2. The 28K temperature rise is consistent with adiabatic temperature rise predictions. The definitions in Equation 3-2 are the same as in Equation 3-1 except that the temperature rise is assumed to be instantaneous.

Equation 3-2

$$T = T_a + \left(T_0 - T_a + \Delta T\right)e^{-\beta t}$$

15 minutes after Shot 121461, the winding pack temperature is estimated to be 98K, well above the assumed pre-shot temperature of 89K. In order to cool down in 15 minutes without further thermal ratcheting, the starting temperature would need to be 95K with a coolant temperature of 80K per this simple model.

The ANSYS code was run to determine what temperature the winding pack would ratchet up to assuming an 80K coolant temperature and a 15 minute pulse repetition rate. The results are shown in Figure 3-9.

The average conductor temperature is predicted to ratchet up to 92K after approximately six shots. No issues are apparent with starting a shot at this higher operating temperature.
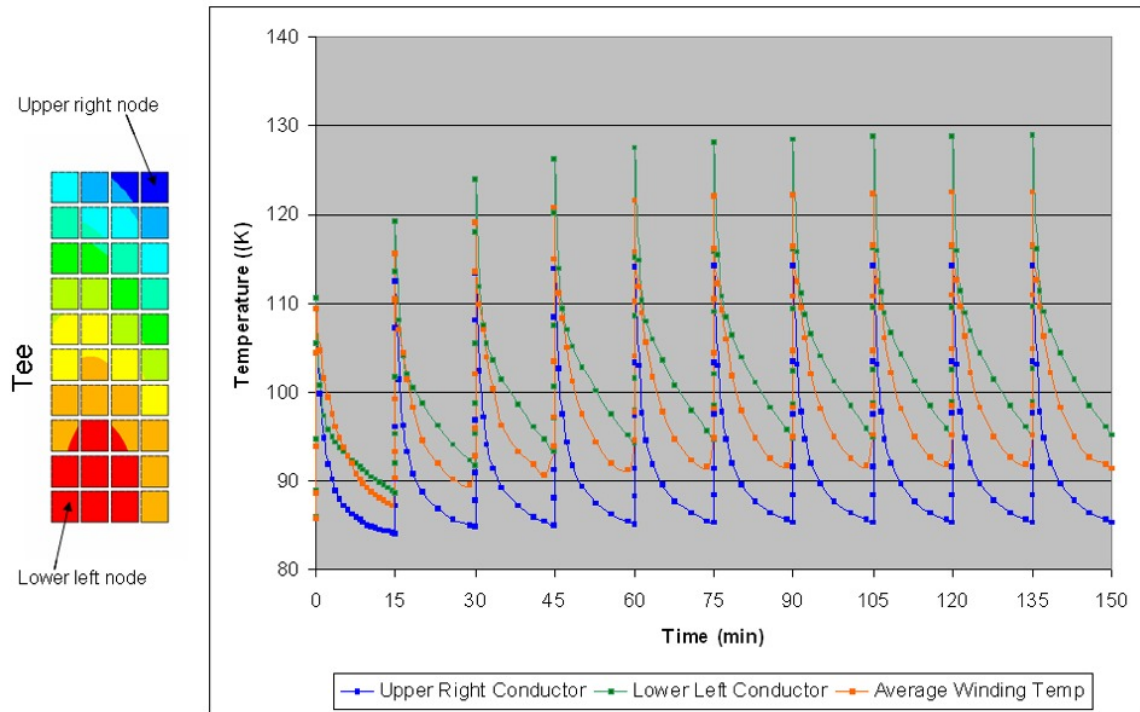

Figure 3-9 Evolution of conductor temperature during continual pulsing

3.3.2   Deflection Measurements

A deflection monitor (aka the deflect-o-meter) was installed to measure deflections across the winding form (approximately a 6' span) during a shot. The design and placement of the deflect-o-meter is shown in Figure 3-10. The deflect-o-meter had a digital output that was recorded on a video camera during the test shots. Deflections measured by the deflect-o-meter were compared with the deflections calculated from an ANSYS model of a single Type C coil for a 36.5kA shot. Both electromagnetic (EM) loads and thermal loads were applied to the ANSYS model. The thermal growth of the winding pack tends to increase deflections whereas the deflections due to EM loads are much larger and in the opposite direction. Therefore, the maximum change in deflection should be experienced around the start of flattop when the thermal growth is least. Graphically, the comparison between the ANSYS deflection (as a function of differential strain) and the average experimental results for the 36.5kA shots are shown in Figure 3-11 (where the differential strain is shown as a positive value). At the differential strain of -112$\mu\varepsilon$ calculated for Shot 121461 (ref. Section 5.2.2.2.2), the predicted deflection of 0.236mm (interpolated from Table 3-2) and the measured maximum deflection of 0.232mm match with 2%, which is well within the error bars of the measurement.

16

Box Dimensions are 94" X 116.5"
ID with wall thickness of 6"

Three tubes

1. 10 foot outer tube ss tube,
   .875 OD, .675" ID.
   (purchased)

2. 12 inch ss tube (box entrance)
   .75" OD, .6875" ID

3. 11 foot inner ss tube ¼
   diameter

Three angles

(2" X 3" 0.1875 thick). These are
from local boat supply store.
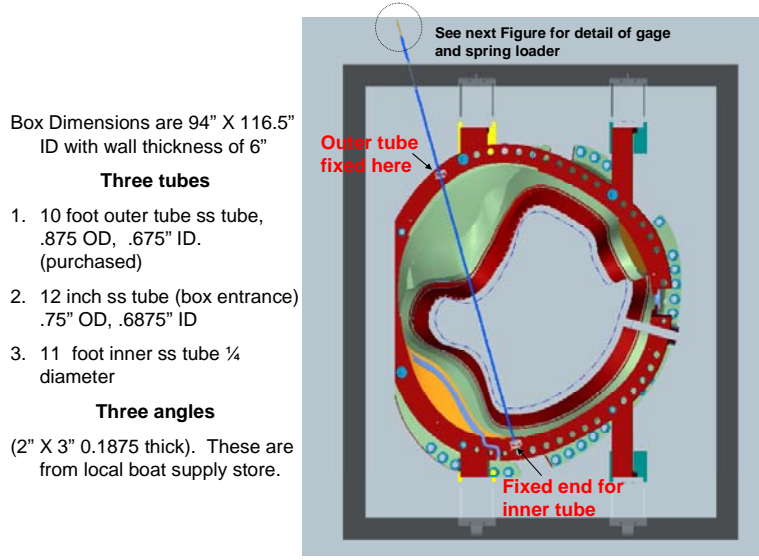
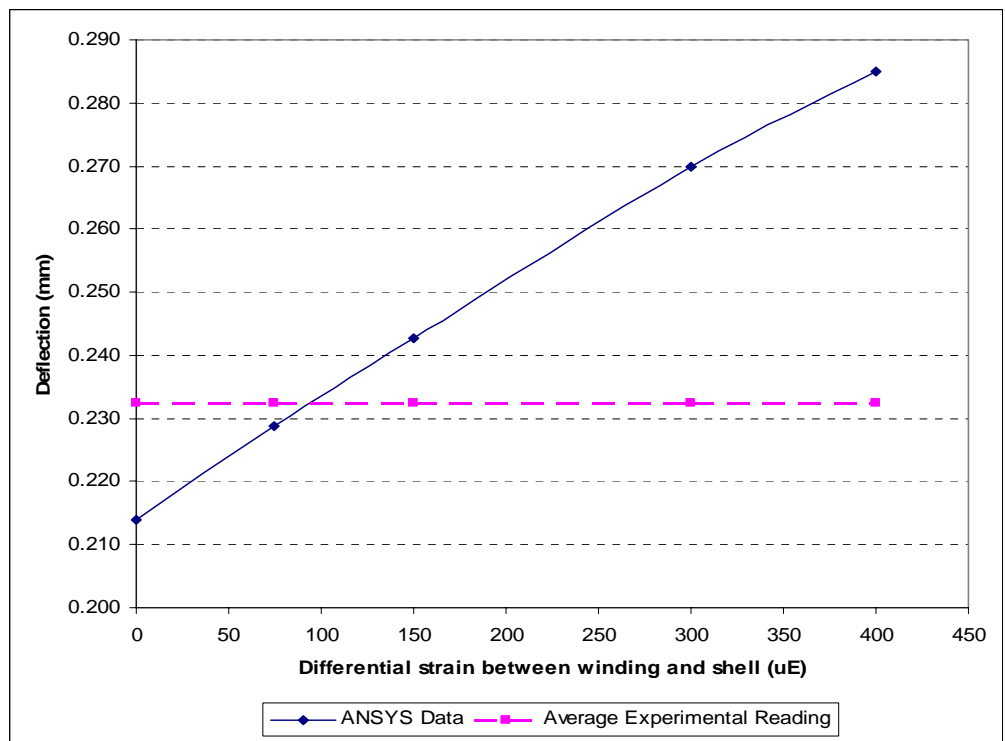**Figure 3-10 Design and placement of the Deflect-o-meter**

Figure 3-11 ANSYS data v. differential strain

Table 3-2 ANSYS and experimental deflection comparison

Calculated deflections (36.5 kA)					Max measured deflections (36.5 kA)		
-0 µε	-75 µε	-150 µε	-300 µε	-400 µε	Shot 121439	Shot 121453	Shot 121461

mm	0.214	0.229	0.243	0.270	0.285	0.239	0.226	0.232

3.3.3 Strain Gage Measurements

Strain gages were installed to measure strains, especially during a pulse when the peak strains which are due to EM loads are present. Comparing thermal strains to predictions is difficult because of the lack of thermocouple measurements in the vicinity of the strain gages. K. Freudenberg carefully reviewed the strain gage data. The results are provided in Section 5.4. The main conclusion was that the strain gage measurements are suspect and not usable. Supporting observations include the following:

- Room temperature data is very scattered when an applied voltage is present whereas the cryogenic data is highly linear.

- The room temperature data becomes smooth when the power supply trips, i.e. when there is no applied voltage but still substantial current. Even the cryogenic data is smoother after the trips.

- The programmed current waveforms are linear. On first principles, the strains due to EM loads should be quadratic with current. Instead, the strains appear linear with current, especially at cryogenic temperatures.

- Strain readings in orthogonal directions at the same approximate location give roughly the same strain due to EM loads. Data does not match ANSYS in direction or magnitude except at gage 15 which is in the lowest field region.

Examination of the voltage and current traces shows that the voltage ripple is extreme. For a nominal 100VDC, the observed voltage ripple was +/-200V. This might explain why the scatter in the room temperature data went away following a power supply trip. Constantan is used in the strain gages and is known to exhibit magneto-resistive properties, especially at cryogenic temperatures. This might explain why the magnitude and temporal profile of the strain measurements were so different from first principle expectations and ANSYS predictions. Recall that the measured displacement was consistent with ANSYS predictions. The implication is that the project needs to qualify a system for monitoring strain which is immune from power supply ripple and magnetic field effects.

4   CONCLUSIONS

- The coil resistance, the observed temperature rise, and the cooldown rate were all in agreement with predicted values.

- Displacements across the width of the coil were measured with a displacement gage and were also in agreement with predicted values.

- Test data from the conventional strain gages used for the C1 tests did not provide usable data. Strain gages which are immune to voltage ripple and magnetic field effects should be further investigated for project use.

- Careful attention should be given to the design of the cryostat cooling system to ensure that the coil cooldown requirement of 96 hours can be met.

5 REFERENCE MATERIAL

5.1   Reference Tables and Figures

Table 5-1 Thermocouple descriptions

Channel # Assignment	Thermocouple ID	Shell Hole number	Side	Location	Comments
Ch 1-bad	TC1_1A_CS	74		casting	
2	TC2_1B_CS	74		casting	
3	TC3_2A_CS	18		casting	
	TC4_2B_CS	18		casting	
	TC5_TCA				Supply Pipe
	TC6_TCB				Supply Outboard Pack
4	TC7_TCC				Supply Inboard Pack
	TC8_TCD				Return Outboard Pack
5	TC9_TCE				Return Outboard Pack
	TC10_TCF				Return Outboard Pack
	TC11_TCG				Return Outboard Pack
	TC12_TCH				Return Inboard Pack
	TC13_TCI				Return Inboard Pack
	TC14_TCJ				Return Inboard Pack
	TC15_TCK				Return Inboard Pack
	TC16_TCL				Return Lead Sides
6	TC17_PACK	85			Winding Pack
7	TC18_CHMBR				Chamber Temp
	TC19				
	TC20				

Table 5-2 Strain gage descriptions

S-Gage chan #	Strain Gage ID	Shell Hole number	Side	Location	Measuring Direction
1	SG1_7A_WP_W	7	A	winding pack	Winding direction
2	SG2_7A_CS_W	7	A	casting	Winding direction
3	SG3_7A_WP_X	7	A	winding pack	Transverse direction
CH 4 bad	SG4_14A_CS_W	14	A	casting	Winding direction
5	SG5_33A_CS_X	33	A	casting	Transverse direction
6	SG6_68B_WP_W	68	B	winding pack	Winding direction
7	SG7_68B_CS_W	68	B	casting	Winding direction
8	SG8_68B_WP_X	68	B	winding pack	Transverse direction
9	SG9_68B_CS_X	68	B	casting	Transverse direction
10	SG10_50B_CS_W	50	B	casting	Winding direction
11	SG11_50B_CS_X	50	B	casting	Transverse direction
12	SG12_50B_WP_W	50	B	winding pack	Winding direction
13	SG13_42A_CS_W	42	A	casting	Winding direction
14	SG14_68A_CS_W	68	A	casting	Winding direction
15	SG15_NLA_CS_P	Near Leads	Near A	Casting	Perpendicular to lead holes
16	SG16_7A_WP_W	7	Redunanat for gage # 1		
17	SG17_7A_CS_W	7	Redunanat for gage # 2		
18	SG18_68B_WP_W	68	Redunanat for gage # 6		
12	SG19_68B_CS_W	68	Redunanat for gage # 7		
20	SG20_42A_CS_W	42	Redunanat for gage # 13		

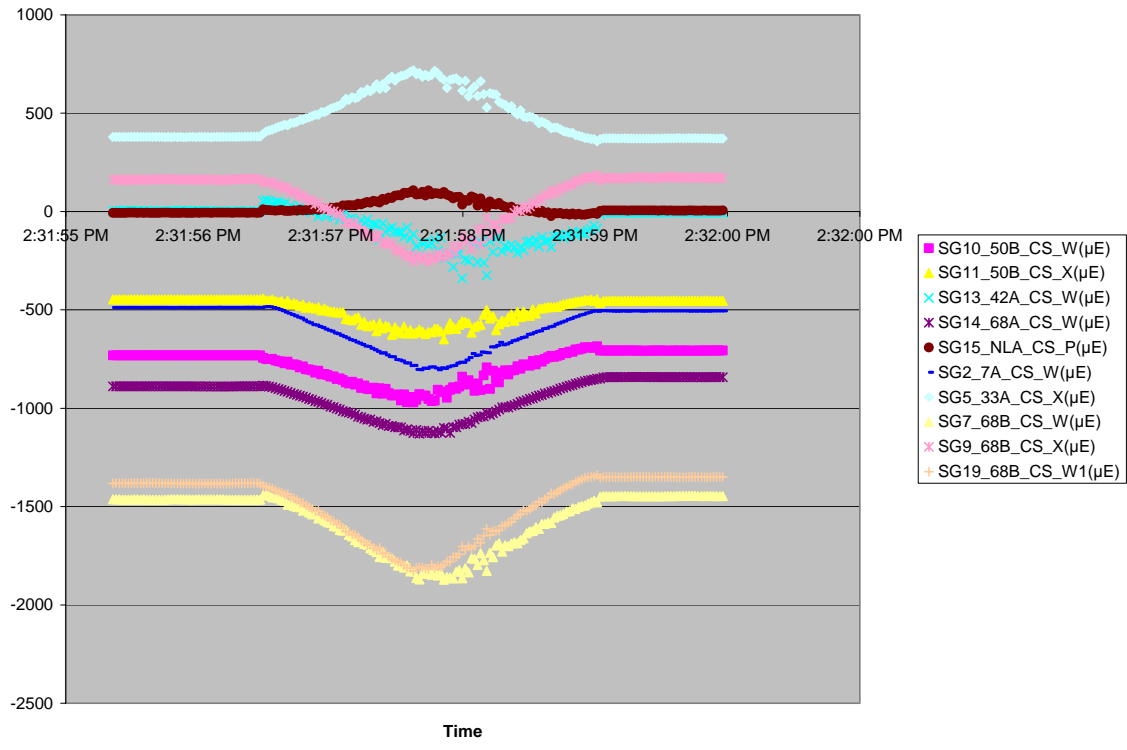Strain gages in gray-scale rows not installed

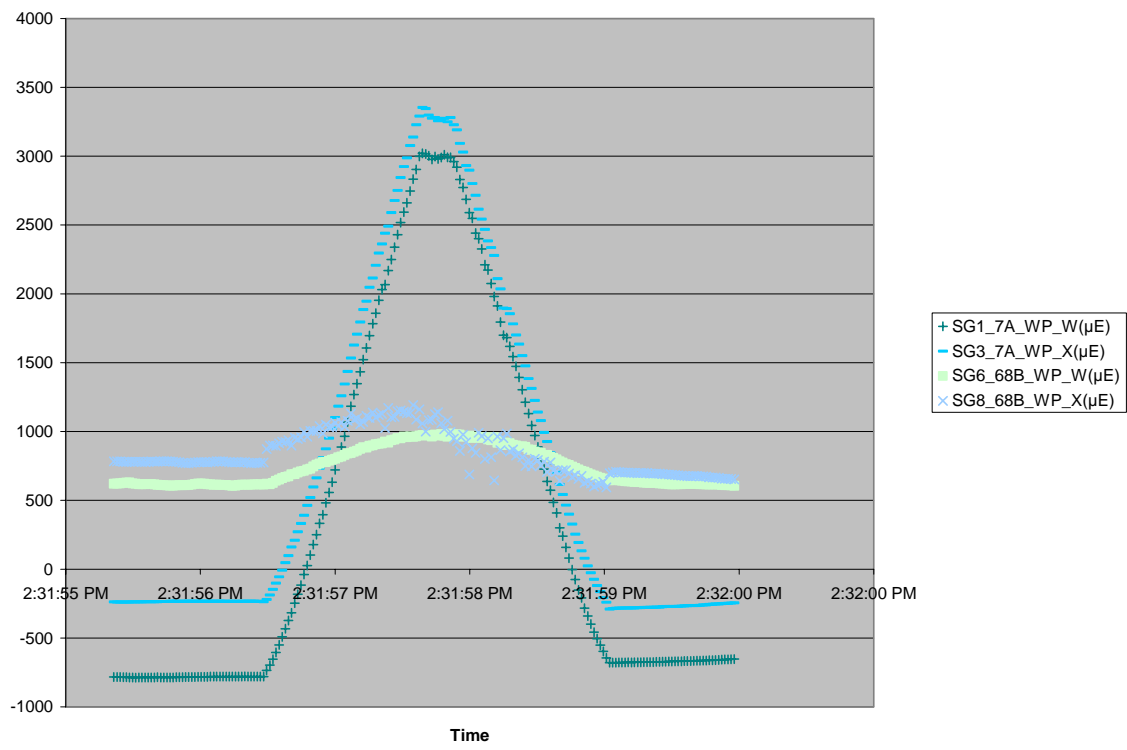**Figure 5-1 Strain gage data for Shot 121461 for strain gages mounted on the winding form**

Figure 5-2 Strain gage data for Shot 1212461 for strain gages mounted on the winding pack

TEMPERATURE COEFFICIENT OF RESISTANCE
FOR BONDABLE RESISTORS

NICKEL - Pure nickel has the highest resistance-versus-temperature sensitivity of the three most commonly used materials and is normally selected for span-versus-temperature compensation of transducers. The temperature coefficient of resistance is +0.33% per deg Fahrenheit (+0.59% deg Celsius) over a temperature range of +50 to +150 deg Fahrenheit (+10 to +65 deg Celsius).

BALCO - With a lower temperature coefficient of resistance (TCR) and a higher resistivity than nickel, Balco yields higher resistance values more easily. The TCR for Balco is +0.24% per deg Fahrenheit (+0.43% per deg Celsius) over the temperature range of +50 to +150 deg Fahrenheit (+10 to +65 deg Celsius).

COPPER - Pure copper has the lowest and most linear TCR, as well as the lowest resistivity of the three materials, making it ideal for smaller scale temperature compensations in transducers. The TCR for pure copper is +0.20% per deg Fahrenheit (+0.36% per deg Celsius).
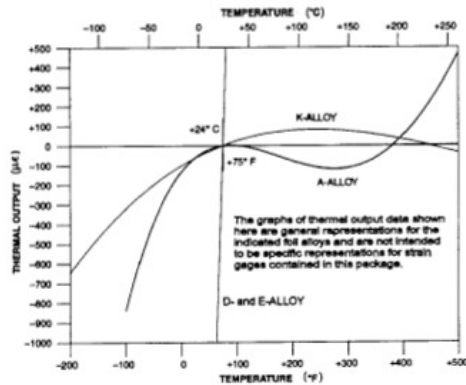
CALCULATION OF THERMAL OUTPUT
FOR STRAIN GAGES

The thermal output of the gages contained in this package can be calculated from the following polynomial expression

$$a_0 + a_1 \cdot T + a_2 \cdot T^2 + a_3 \cdot T^3 + a_4 \cdot T^4$$

where aN are the coefficients and T^N is temperature to the Nth power.

The coefficients for both Celsius and Fahrenheit temperature scales are provided on the data label affixed to this package for strain gages.

A-Alloy, D-Alloy, and E-Alloy will generally use all five coefficients (a0 to a4) but K-Alloy will generally use only the first four coefficients (a0 to a3) with the fifth (a4) being zero.

VISHAY. VISHAY MICRO-MEASUREMENTS & SR-4
Magnetic Field
STRAIN GAGES

FOR COMPLETE TECHNICAL DATA, VISIT WWW.VISHAY.COM/REF/STRAINGAGES

GRID RESISTANCE IN OHMS	T.C. OF GAGE FACTOR, %/100°C
700.0±0.5%	(+1.3±0.2)

GRID	GAGE FACTOR AT 24°C	TRANSVERSE SENSITIVITY
1	2.105±0.5%	(+0.6 ±0.2)%
2		
3		
NOM		

THERMAL OUTPUT COEFFICIENTS FOR 1018 STEEL

ORDER	FAHRENHEIT	CELCIUS
0	-1.19E+2	-4.11E+1
1	+3.22E+0	+3.12E+0
2	-2.62E-2	-6.61E-2
3	+6.31E-5	+3.40E-4
4	-3.75E-8	-3.94E-7

FOIL LOT NUMBER	BATCH NUMBER
A44AD25	F374099

ITEM CODE	QUANTITY	CODE
7856	5	151321

MADE IN UNITED STATES

H06A-AC1-125-700

Technical notes from Vishay on strain gage technology can be found at the following URL:

http://www.vishay.com/brands/measurements_group/guide/indexes/tn_index.htm

Figure 5-3 Calculation of thermal output for strain gages

SIZE / MODEL	.5 x .5 x 3		AC30	PUMP PERFORMANCE CURVE
APPLICATION	TRANSFER			CURVE NO. P04-10507A-1
DRIVE	DIRECT			
CUSTOMER	PRINCETON LABS			PUMP RPM 5800
PROJECT/ITEM NOS.	0			LN2 0.809
FSCM NO. 15275	CONDITIONS	7 GPM	86 FEET	IMPELLER DIA." 3.00

Pump operating flow range is 3 to 8 gpm. Shut down pump if differential pressure drops below 22 psi.

Maximum allowable motor current is 3.7 amps (460 vac, 3 hp).

Always provide clean, dry product with adequate NPSH to the pump suction.
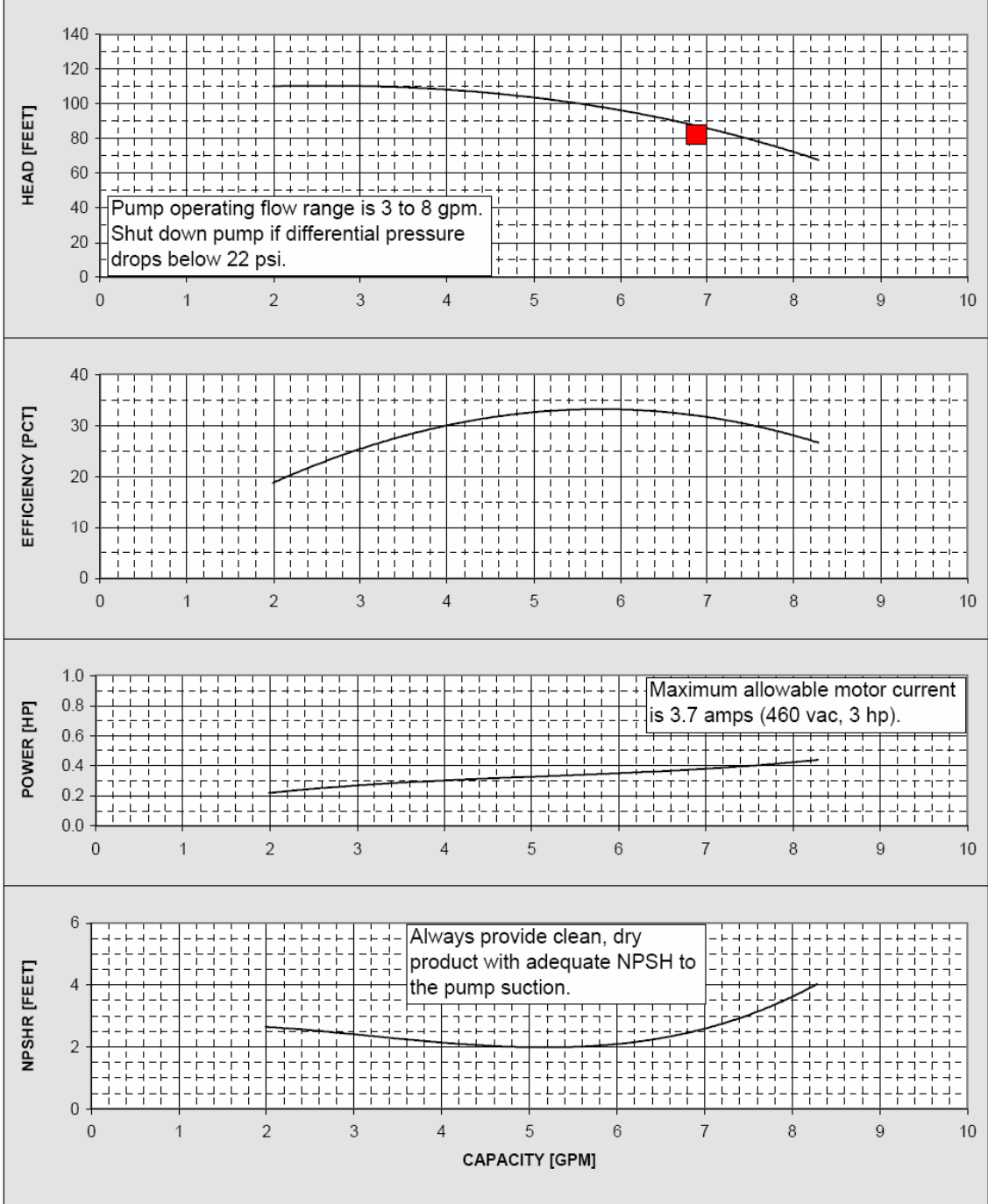
Figure 5-4 Pump performance curve

24

5.2   Deflection Measurements and Analysis[2]

5.2.1   Introduction

The objective of this task is to validate the finite element model of the NCSX C1 coil built in ANSYS with the experimental data taken doing the cryogenic magnetic testing of the first Type C modular coil. The C1 Coil test was performed at PPPL doing late June 2006.

The purpose of this analysis is to examine the structural characteristics of the NCSX modular coil (C1) and windings. The modular coils provide the primary magnetic field within NCSX and consist of flexible cable conductor wound on a cast and machined winding form and vacuum impregnated with epoxy. Eighteen coils and associated winding forms are connected at assembly into a toroidal shell structure. The ANSYS model for the complete NCSX analysis includes the complete shell structure of all three coils and contact regions allow the winding to slide and detach form the shell structure. The winding pack is thus restrained only by the clamps. This analysis only considers the C1 coil with the only loading derived from the windings on the C1 shell casting.

5.2.2   Modeling

The geometry of the shell and windings renders any global stress analysis performed by hand as a virtual impossibility. Thus, the approach taken in this report was to perform a series of finite element models and compare and contrast the answers while varying certain parameters namely the differential thermal strain between the winding pack and the casting.   The finite element model built in ANSYS is shown in Figure 5-5below. It includes the C1 casting, two winding packs, clamps, clamp pads and the support legs that held the casting above the floor. In the model and in the experiment the B side of the coil is pointed upward away from the floor.
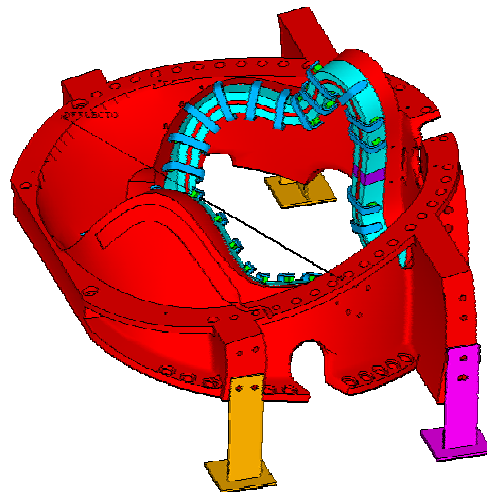

Figure 5-5 Finite element model for the C1 coil

5.2.2.1   Material Properties and Assumptions

Assumptions are as follows:

a.   Material properties evaluated at 77 K.

b.   Winding packs are modeled with isotropic material properties.

---

[2] Provided by K. Freudenberg (ORNL)

c.   Non-linear sliding between tee and winding pack is frictionless.

The properties used assumed that the shell is made of stainless steel and the coil windings consist of a homogeneous copper/epoxy mixture. The properties are listed in Table 5-3 and are derived from a paper by Leonard Myatt, "Material Property Data Base to be used for NCSX Analysis", June 2004.

Table 5-3 Material properties

Component	Material	Modulus (GPa)	Poisson's ratio
Tee/Shell Casting	Cast Stainless Steel	159	0.31
Modular Coils	Copper Epoxy mixture	59	0.3

5.2.2.2   Loading

5.2.2.2.1   Magnetic Loads

The magnetic model of the windings was solved in ANSYS for 36.5 kA corresponding to the 2T high Beta scenario. The corresponding nodal forces on the coils are then transferred to the structural model in order to determine strain and deflection. Figure 5-6 through Figure 5-9 show the radial and lateral loading for both winding packs (C1 by itself, no other magnetic fields are included). An independent magnetic analysis performed by Art Brooks of PPPL shown in the upper right of each of the figures demonstrates that ANSYS and independent model are in very good agreement with the force loading predicated.
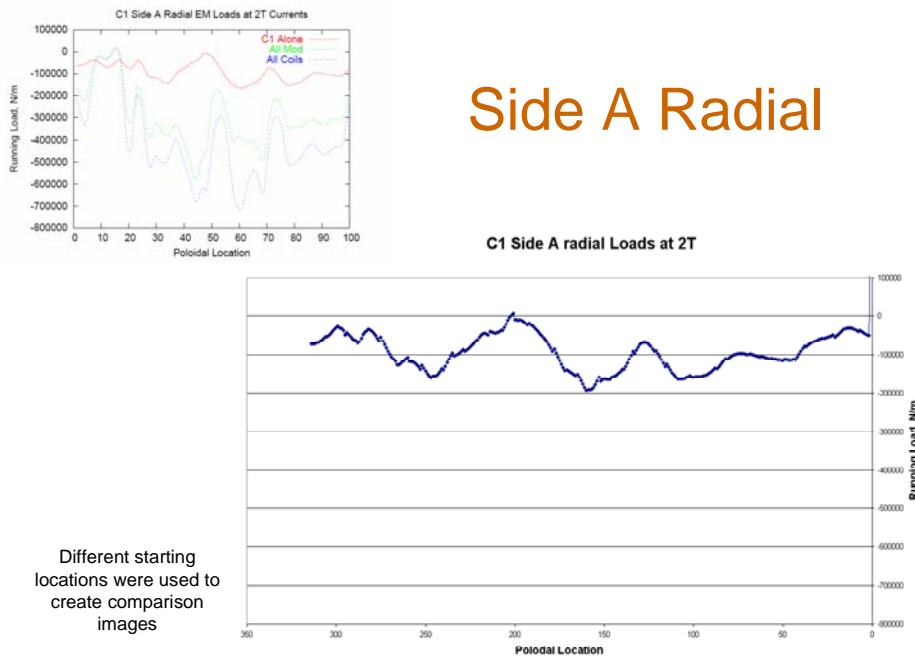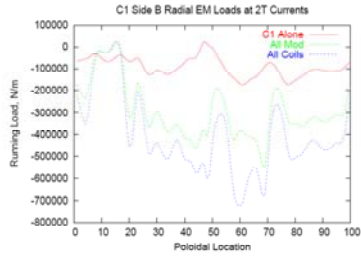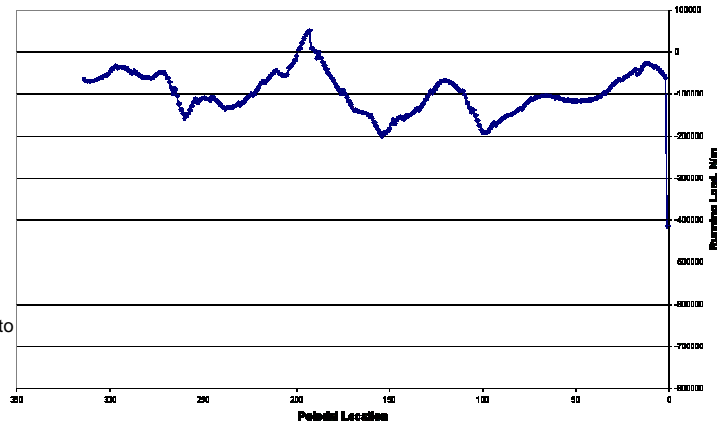

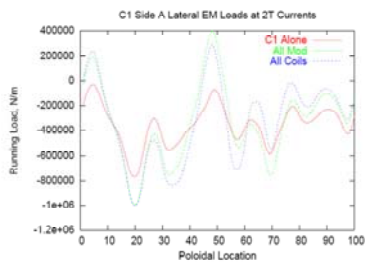**Figure 5-6 Radial loading comparison for Side A winding pack**

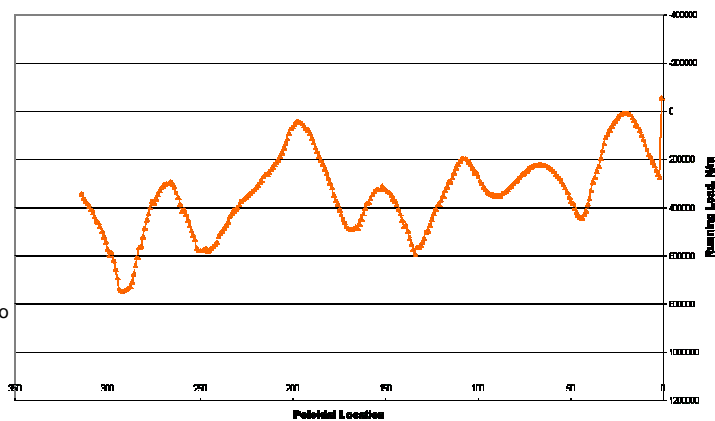## Side B Radial

C1 Side B radial Loads at 2T

Different starting locations were used to create comparison images

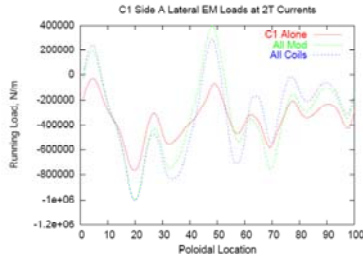**Figure 5-7 Radial loading comparison for Side B winding pack**

Side A Lateral

C1 Side A Lateral Loads at 2T

Different starting locations were used to create comparison images

Figure 5-8 Lateral loading comparison for Side A winding pack

C1 Side A Lateral Loads at 2T

Side A Lateral

Different starting locations were used to create comparison images
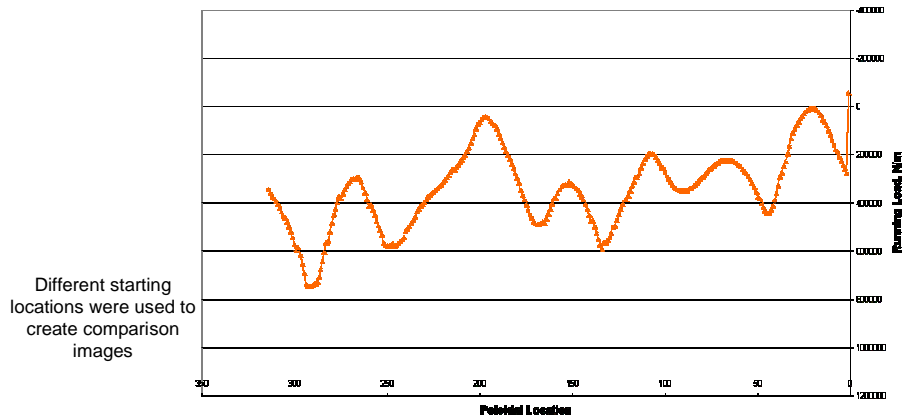
Figure 5-9 Lateral loading comparison for Side B winding pack

5.2.2.2.2   Thermal loads

The winding experiences about 0.023 % shrinkage more than the shell when being cooled down from room temperature to 80K as shown in Figure 5-10. During the tests, there was a significant temperature difference between the winding and the shell. For Shot 121461, the starting temperature of the winding pack was approximately 84K whereas the shell temperature was approximately 95K. During a shot, the winding pack temperature rises adiabatically by 28K whereas the shell temperature remains constant. Therefore, the differential thermal strain changes from -226$\mu\epsilon$ at the start of the pulse, to -112$\mu\epsilon$ at the start of flattop, to   -41$\mu\epsilon$ at the end of the flattop, and to +80$\mu\epsilon$ at the end of the pulse. As shown in Table 5-4, the thermal growth of the winding pack tends to increase deflections whereas the deflections due to EM loads are much larger and in the opposite direction. Therefore, the maximum change in deflection should be experienced around the start of flattop when the differential strain is estimated to be -112$\mu\epsilon$.
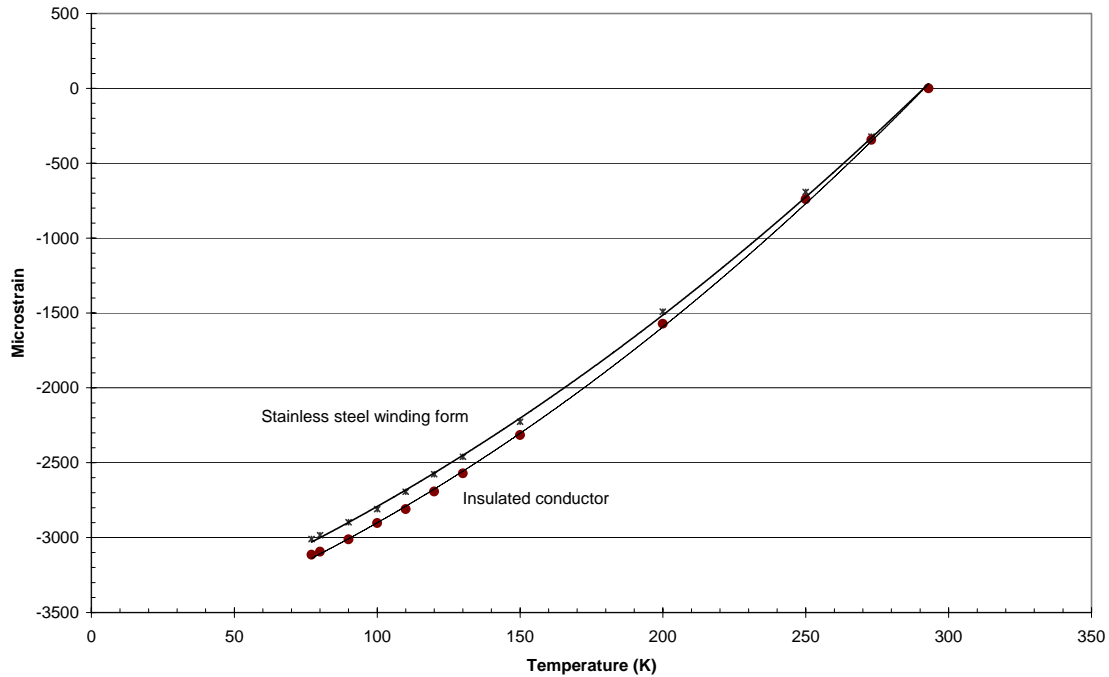
Figure 5-10 Thermal contraction of the winding form and conductor

5.2.2.3 Restraints and Mesh

The finite element model is restrained in a similar manner to the experimental coil as shown in Figure 5-11. One leg was held fixed to the floor and the other legs were free to slide. Initially, the sliding legs were held to the floor and allowed only to slide along the floor and not lift up off the floor. After reviewing the first sets of deflection slides, it was determined that the magnetic field tended to lift one of the legs off the floor. This leg was then this released in the model since the experiment did not have any device that would restrain this type of movement. The ANSYS mesh (shown in Figure 5-11) consists of both tetrahedral shell elements and hexahedral coil elements. Bonded contact surfaces are used to join all parts together. The contact surfaces between the windings and the shell structure are set to a frictionless option so that the coil may be "slippery" and slide along the length of the coil, as well as open up gaps from the shell. Although some features have been suppressed in the shell, namely bolts holes on the flanges, there are many intricate details that are incorporated in the shell structure. These include the tee relief grove, port holes, and various other chamfers, rounds and cuts which provide for a very robust model and mesh. The winding pack mesh consists of a 2 X 6 element formulation with an average element length of 2.3 cm.
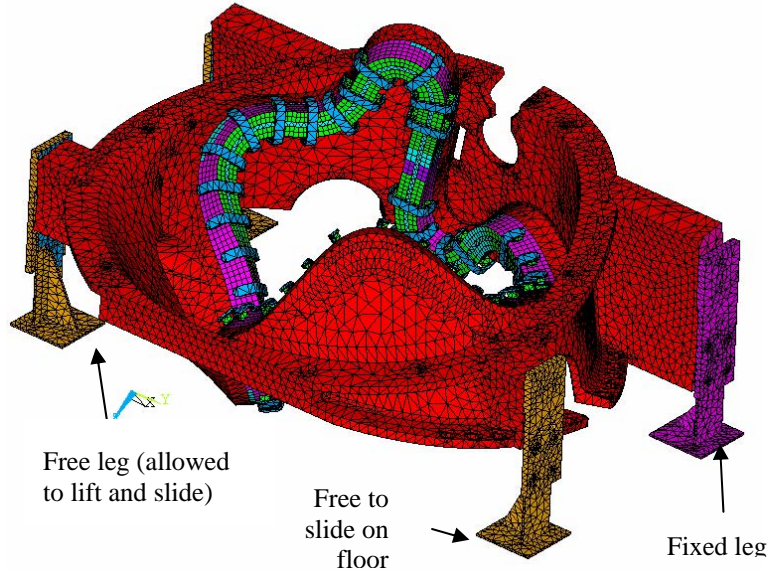
29

Free leg (allowed to lift and slide)

Free to slide on floor

Fixed leg

Figure 5-11 Restraints and mesh of the C1 Coil

5.2.3   Design and Placement of the Deflect-o-meter

The deflect-o-meter general schematic is shown below in Figure 5-12. It consists of two concentric stainless steel tubes; several support brackets; and a dial indicator. The outer tube is fasted to one side of the coil and the inner tube is spring loaded to push against the other side of the coil via a bracket while sliding in the outer tube. A final tube is needed to allow sliding through the cryostat chamber. The actual location of the deflect-o-meter varies slightly from the figure below as the lower connection point, where the inner tube is pushing, is farther to the right than shown.
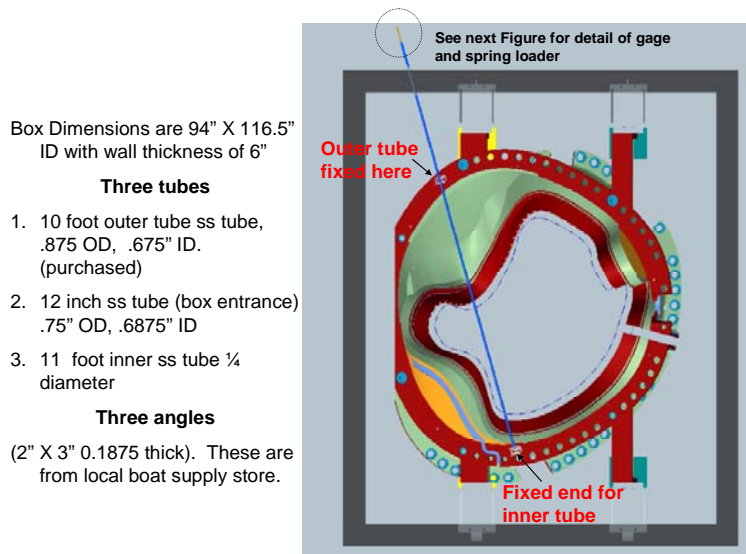

Box Dimensions are 94" X 116.5" ID with wall thickness of 6"

Three tubes

1. 10 foot outer tube ss tube, .875 OD, .675" ID. (purchased)

2. 12 inch ss tube (box entrance) .75" OD, .6875" ID

3. 11 foot inner ss tube ¼ diameter

Three angles

(2" X 3" 0.1875 thick). These are from local boat supply store.

See next Figure for detail of gage and spring loader

Outer tube fixed here

Fixed end for inner tube

Figure 5-12 Schematic of the installation of the deflect-o-meter

The dial indicator is installed according to Figure 5-13 using clamp collars, springs, rubber bellows and zip ties. The indicator is mounted on the outer tube and reads positive from left to right in the figure. Therefore, if the coil expands (the mount points move further apart on the coil) the inner tube will move closer to the gage and the reading will be negative. Likewise, if the coil contracts, the reading will be positive.

A camera/camcorder was positioned above the dial indicator and recorded at 30 fps (frames per second). The shot pulse had a one second rise time, a 0.2 second flattop and a 1 second decay time. Thus, a total of 66 frames captured the shot but the video had to be analyzed frame by frame to derive the data.
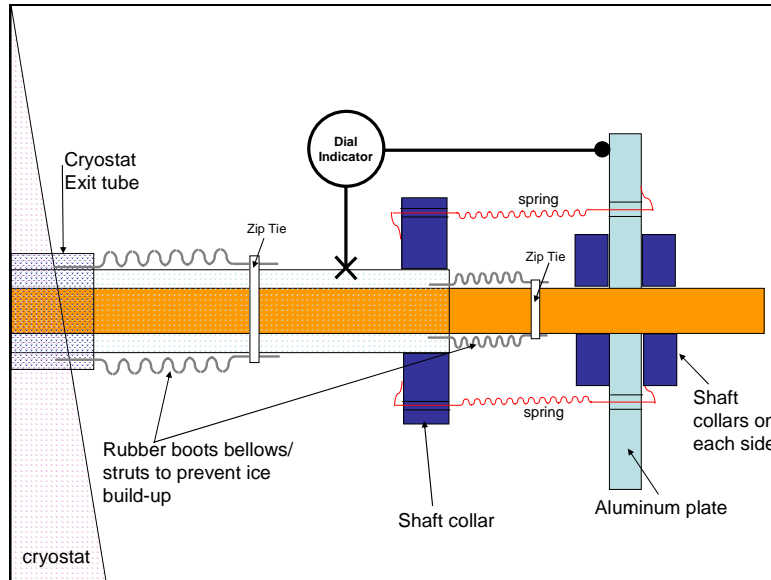
Figure 5-13 Schematic of the installation of the dial indicator installation on the deflect-o-meter

The actual location of the outer tube connection location is shown in Figure 5-14 with the outer tube installed and with the bar removed. The location of the inner tube's placement is shown in Figure 5-15.
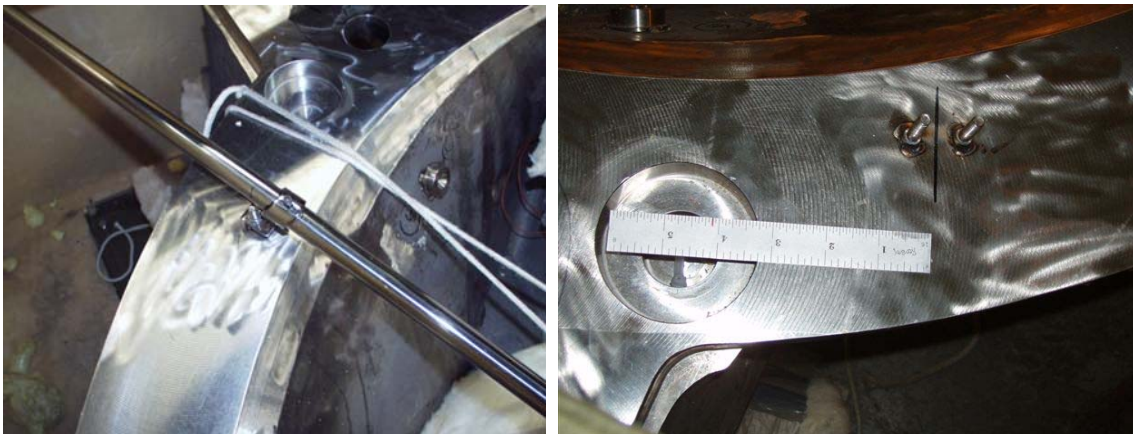

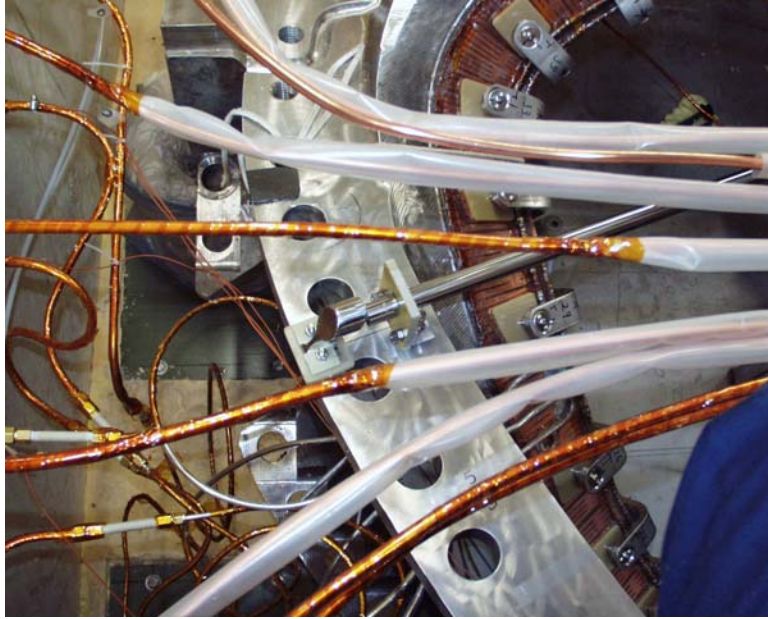**Figure 5-14 Deflect-o-meter installed on C1 coil**

Figure 5-15 Placement of inner deflect-o-meter tube

After reviewing these images the location of the deflect-o-meter in ANSYS was moved accordingly. Figure 5-16 shows the deflect-o-meter as a dashed line located between the two nodes chosen for measurement. Deflection between the two points is measured by aligning a coordinate system in ANSYS between he two points and reading the change in x- direction/position of the two points relative to each other.
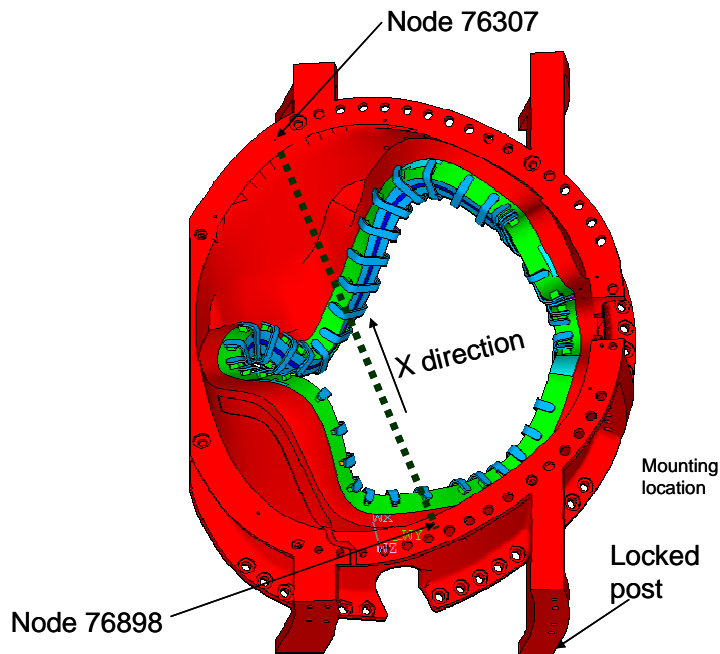

Figure 5-16 ANSYS model for the location of the deflect-o-meter

5.2.4 Comparison between ANSYS and Experimental Results

5.2.4.1 Experimental Results

The deflect-o-meter's video file was analyzed frame by frame for each shot. The results of the peak deflection values for each shot are shown in Table 5-4. The data includes a series of shots at cryogenic temperature (approx 83 K) with a peak current of 36.5 kA and two shots at 15 kA at room temperature. The last two columns in the table are the range of deflection values since the deflect-o-meter rarely returned to its original starting value after a shot. When comparing the warm and cold shots for the 15 kA shots, there does not appear to be an appreciable difference in measurement. They are in the same range which is significant when the strain gage readings (not discussed in this report) are considered. Finally, the repeatability of the deflect-o-meter is estimated to be around 0.008 mm (.0003 in) based on dry run testing performed at ORNL.

Table 5-4 Deflect-o-meter data for shots

			C1 Coil test at PPPL June 2006					Deflection Range	
Shot	Current (Kamps)	Type	Initial (in)	Max (in)	End (in)	Strain difference after shot (in)	Deflection (in)	Deflection (mm)	Deflection including offset after shot (mm)
121405	15	flattop	0.0002	-0.0003	0.0005	-0.0003	0.0005	0.013	0.020
121408	25	flattop	0.001	-0.0029	0.0017	-0.0007	0.0039	0.099	0.117
121412	36	trip	0.002	-0.0029	0.0026	-0.0006	0.0049	0.124	0.140
121416	36	trip	0.0026	-0.0048	0.0031	-0.0005	0.0074	0.188	0.201
121419	36	flattop	-0.0105	-0.0185	-0.0095	-0.001	0.008	0.203	0.229
121426	36	flattop	-0.0089	-0.0179	-0.0084	-0.0005	0.009	0.229	0.241
121439	36	flattop	-0.0097	-0.0189	-0.0093	-0.0004	0.0092	0.234	0.244
121453	36	flattop	-0.0085	-0.0169	-0.0075	-0.001	0.0084	0.213	0.239
121461	36	flattop	-0.0071	-0.0159	-0.0064	-0.0007	0.0088	0.224	0.241
121468	26	flattop	-0.0065	-0.0119	-0.0065	0	0.0054	0.137	0.137
121471	15	flattop	-0.0063	-0.0069	-0.0063	0	0.0006	0.015	0.015
121537	15 (warm)	flattop	-0.0001	-0.0009	0.0002	-0.0003	0.0008	0.020	0.028
121540	15 (warm)	flattop	0.0009	0.0004	0.0017	-0.0008	0.0005	0.013	0.033

Figure 5-17, Figure 5-18, and Figure 5-19 show the deflection as a function of time for three of the 36.5 kA shots. The behavior generally has the trend of a 2nd order polynomial for the rise and decay times, which is expected because of the squared relationship between current and force. Some of the frames were blurred and thus several data points may have been interpreted poorly. Interestingly, the deflect-o-meter does not begin to read until approximately 0.3 seconds have elapsed into the rise time of the currant.
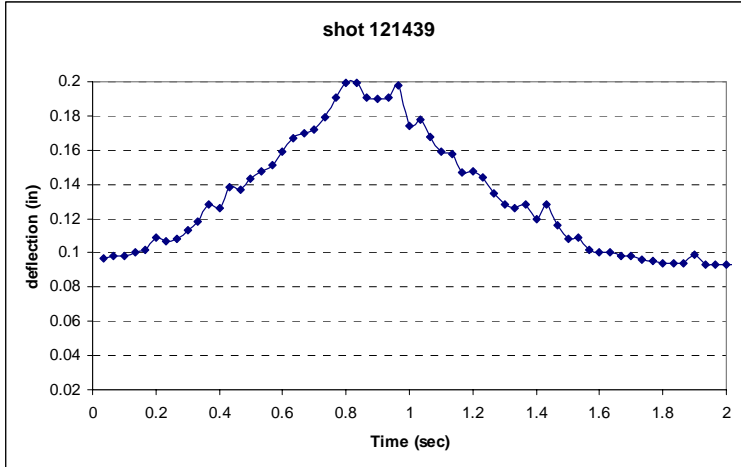
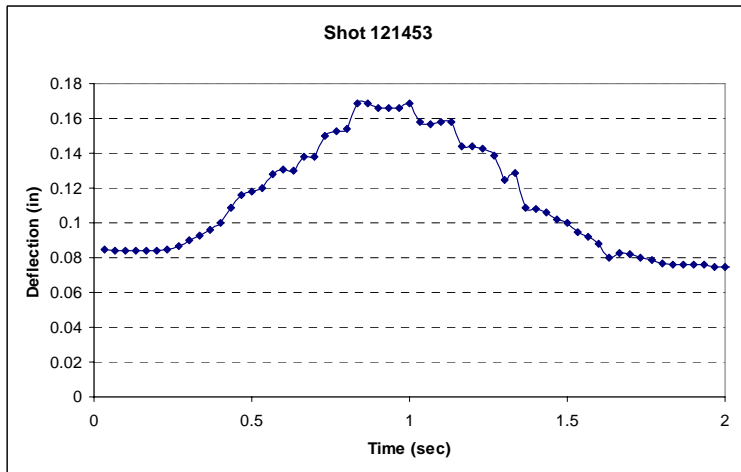**Figure 5-17 Shot 121439 from the deflect-o-meter as a function of time**

Figure 5-18 Shot 121453 from the deflect-o-meter as a function of time
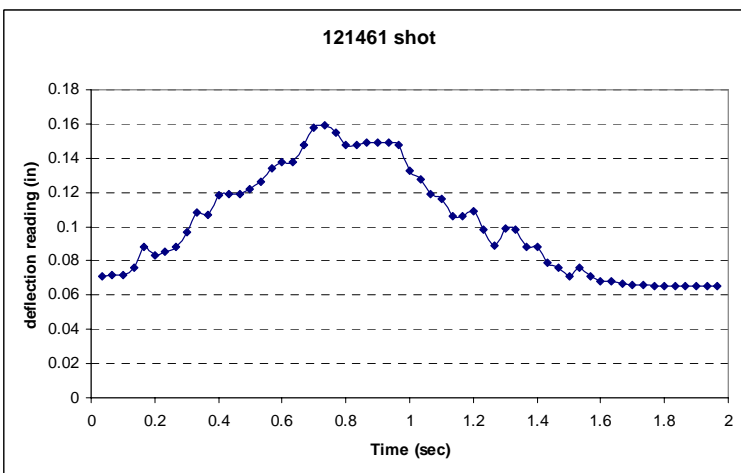

Figure 5-19 Shot 121461 from the deflect-o-meter as a function of time

5.2.4.2   ANSYS Results

After initial examination of the behavior of the casting, it was determined that one of the legs of the casting tended to come off the floor via the magnetic forces. This is illustrated in Figure 5-20 which shows two restraint scenarios where the legs are held to the floor either in all directions or with roller supports.   In both cases, the left front leg (north-west when viewed from above) is treated as always touching the floor. However, the possibility that one leg actually moves up essentially supporting the coil on a tripod must be considered. The magnetic field tends to push that leg off the floor (see the red area on the figure on the right). By supporting it as always in contact with the floor, the coil is forced to move and bend to accommodate that displacement which is clearly an unwanted effect.
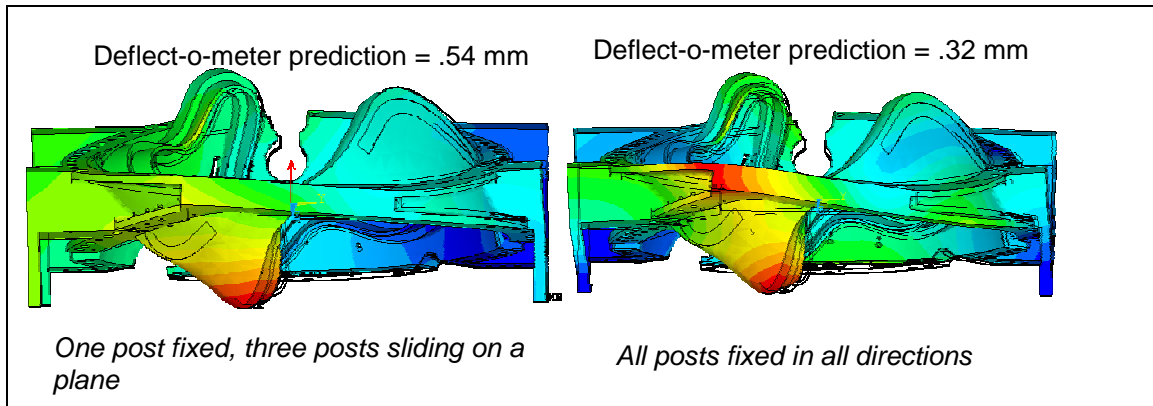
Figure 5-20 Modeling restraints and the effects of magnetic loading one the leg supports

Henceforth, the ANSYS restraint allows the north-west leg to move upward. Figure 5-21 and Figure 5-22 show the deflection profile for the assumed case for the -400 $\mu\varepsilon$ and zero $\mu\varepsilon$ cases respectively. The coil leg moves up 4-5 mm away from the floor for the -400 $\mu\varepsilon$ and 4.5-5.5 mm for the 0 $\mu\varepsilon$ case.
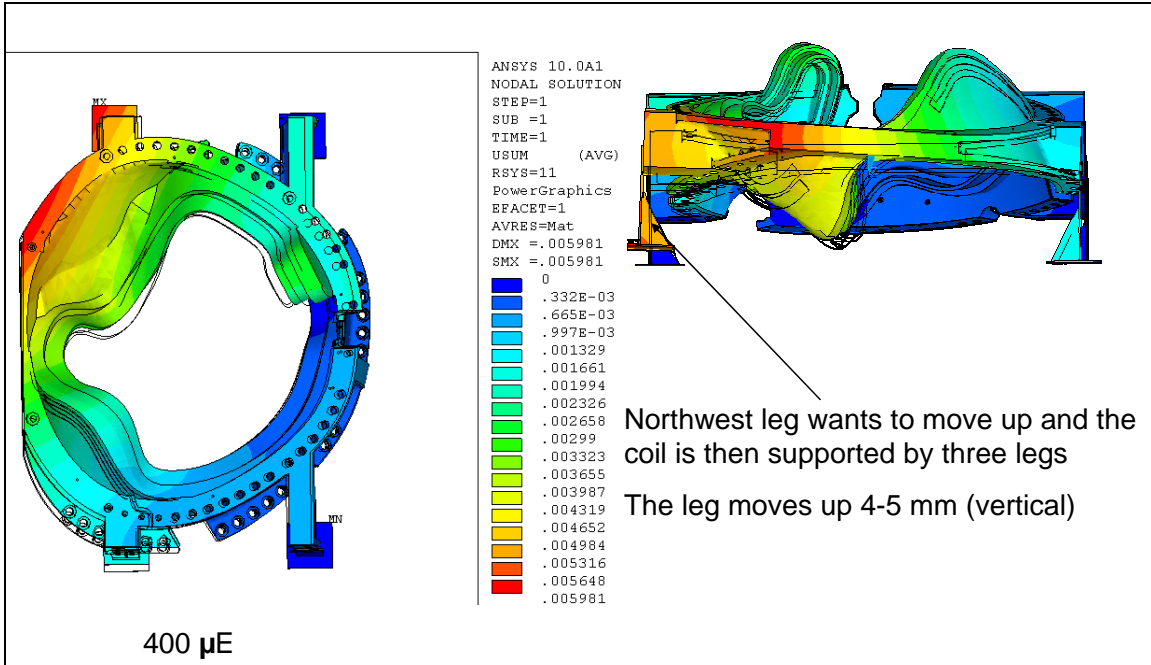
ANSYS 10.0A1
NODAL SOLUTION
STEP=1
SUB =1
TIME=1
USUM   (AVG)
RSYS=11
PowerGraphics
EFACET=1
AVRES=Mat
DMX =.005981
SMX =.005981

	0
	.332E-03
	.665E-03
	.997E-03
	.001329
	.001661
	.001994
	.002326
	.002658
	.00299
	.003323
	.003655
	.003987
	.004319
	.004652
	.004984
	.005316
	.005648
	.005981

Northwest leg wants to move up and the coil is then supported by three legs

The leg moves up 4-5 mm (vertical)

400 **µ**E

Figure 5-21   ANSYS deflection plot illustrating relative movement of coil for -400 µε between coil and winding form

ANSYS 10.0A1
NODAL SOLUTION
STEP=1
SUB =1
TIME=1
USUM   (AVG)
RSYS=11
PowerGraphics
EFACET=1
AVRES=Mat
DMX =.006494
SMX =.006494

	0
	.361E-03
	.722E-03
	.001082
	.001443
	.001804
	.002165
	.002526
	.002886
	.003247
	.003608
	.003969
	.00433
	.00469
	.005051
	.005412
	.005773
	.006133
	.006494

The North west leg moves up 4.5-5.5 mm (vertical)

0 **µ**E
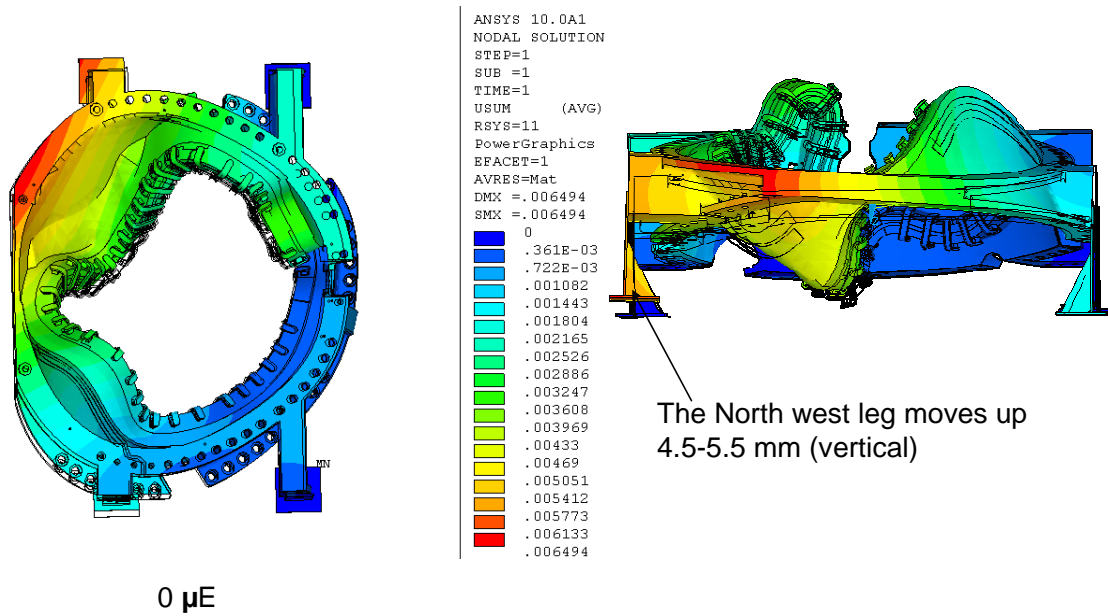
Figure 5-22   ANSYS deflection plot illustrating relative movement of coil for no relative thermal strain between coil and winding form

The deflections calculated in ANSYS between the points where the deflect-o-meter is installed, are shown in Table 5-5. The differential strain between the winding pack and the casting was treated parametrically by assuming values between 0 and -400µε. As discussed in Section 5.2.2.2.2, the differential thermal strain is calculated to change from -226µε at the start of the pulse, to -112µε at the start of flattop, to   -41µε at the end of the flattop, and to +80µε at the end of the pulse. As shown in Table 5-4, the thermal growth of

the winding pack tends to increase deflections whereas the deflections due to EM loads are much larger and in the opposite direction. Therefore, the maximum change in deflection should be experienced around the start of flattop when the thermal growth is least. Graphically, the comparison between the ANSYS deflection (as a function of differential strain) and the average experimental results for the 36.5kA shots are shown in Figure 5-23 (where the differential strain is shown as a positive value). At the differential strain of -112$\mu\epsilon$ calculated for Shot 121461, the predicted deflection of 0.236mm (interpolated from Table 5-5) and the measured maximum deflection of 0.232mm match with 2%, which is well within the error bars of the measurement.

Table 5-5 ANSYS and experimental deflection comparison

	Calculated deflections (36.5 kA)					Max measured deflections (36.5 kA)		
	-0 $\mu\epsilon$	-75 $\mu\epsilon$	-150 $\mu\epsilon$	-300 $\mu\epsilon$	-400 $\mu\epsilon$	Shot 121439	Shot 121453	Shot 121461
mm	0.214	0.229	0.243	0.270	0.285	0.239	0.226	0.232
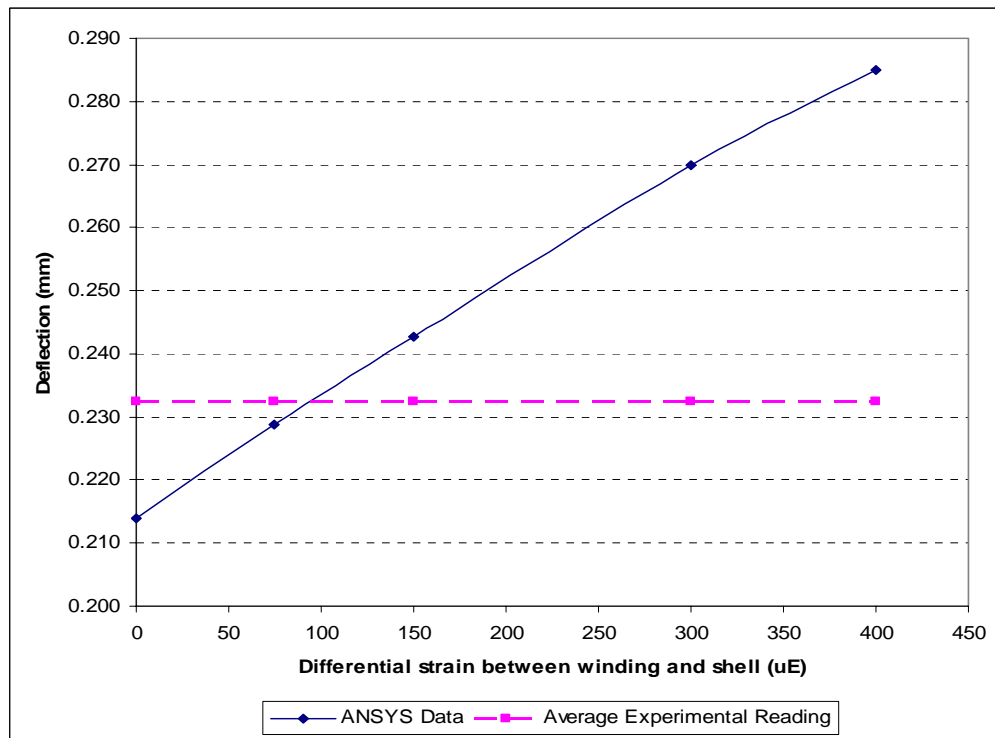
Figure 5-23 ANSYS data v. differential strain

5.3   Photographs of the Test Setup

Figure 5-24 Cryostat carriage in fabrication

Figure 5-25 Cross-section of 4-conductor current feed with fiberglass angle supports
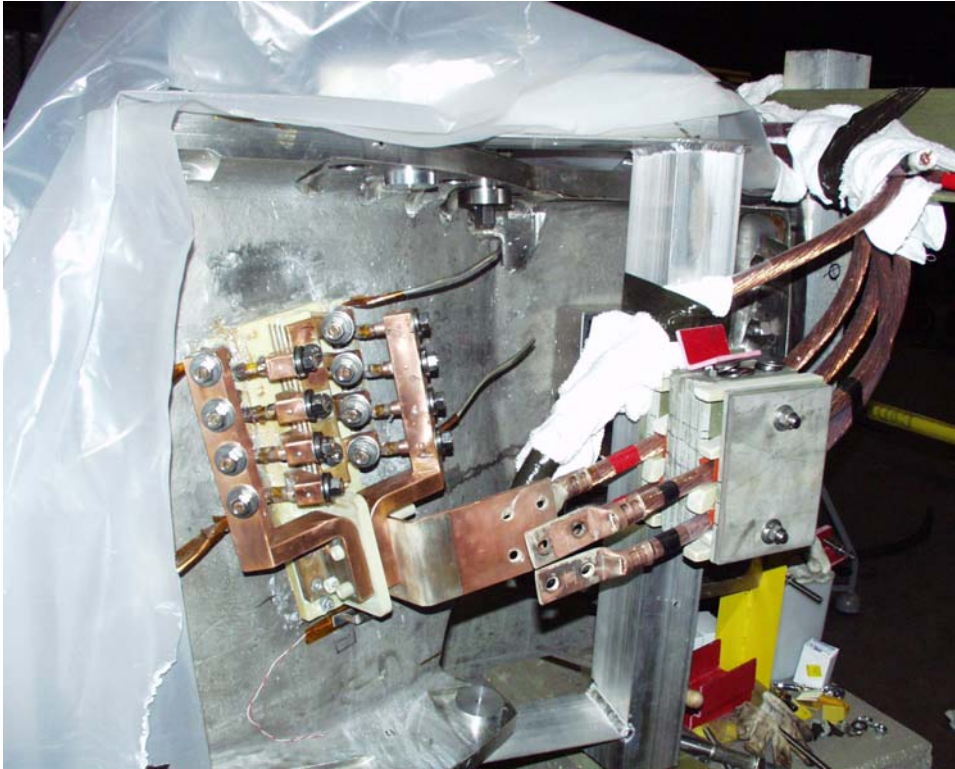
Figure 5-26 Connection of current feed to C1 coil

Figure 5-27 Crimped lugs on current feeds

Figure 5-28 Bus connection to 4-conductor current feed inside thermal transition box

Figure 5-29 Connection of cryostat to facility exhaust

Figure 5-30 Cryostat inside Coil Test Facility
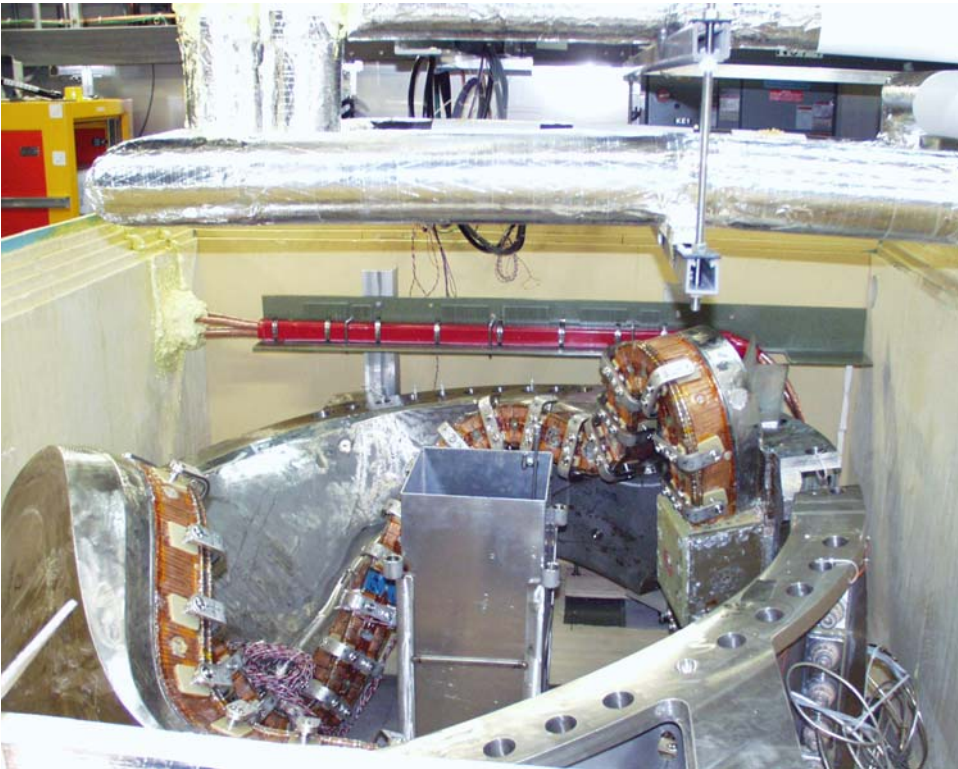
Figure 5-31 C1 coil inside cryostat

Figure 5-32 Restraints on C1 supports
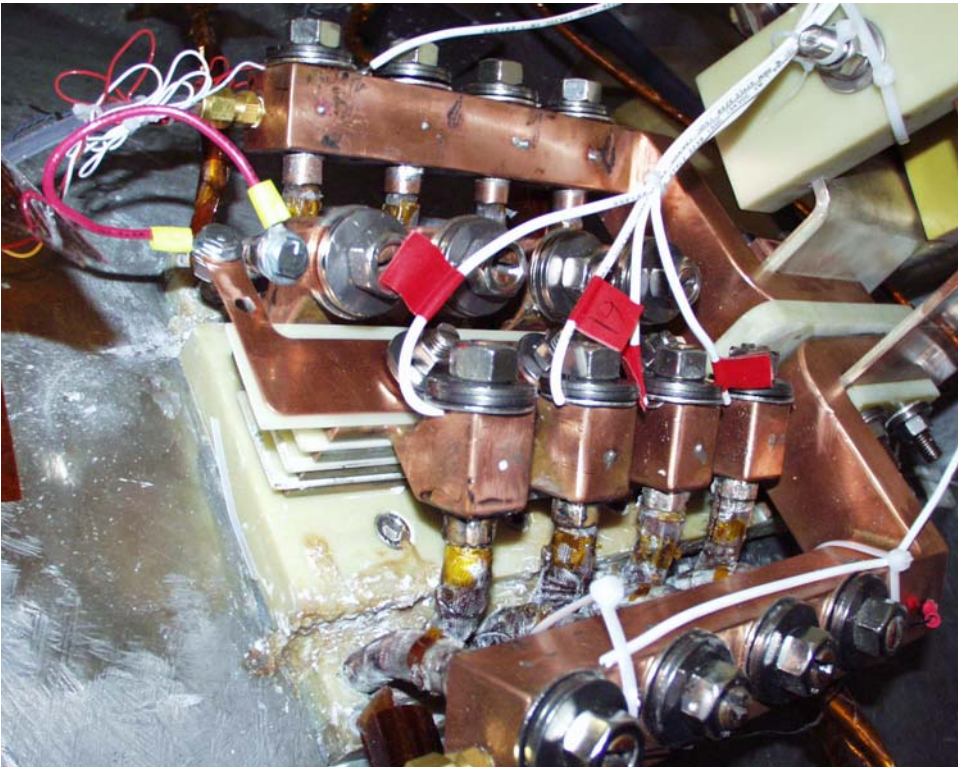
Figure 5-33 Instrumentation of jumper assembly

Figure 5-34 Strain gages at Clamp 68 - Side B

Figure 5-35 Casting strain gages at Clamp 68 - Side B
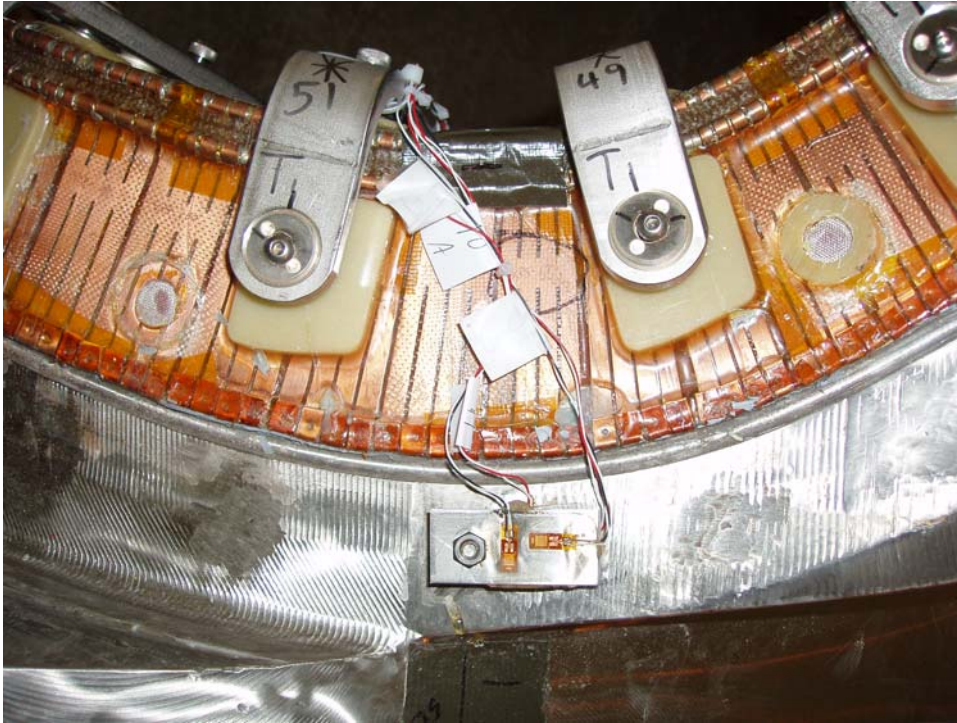
Figure 5-36 Strain gages at Clamp 50 - Side B
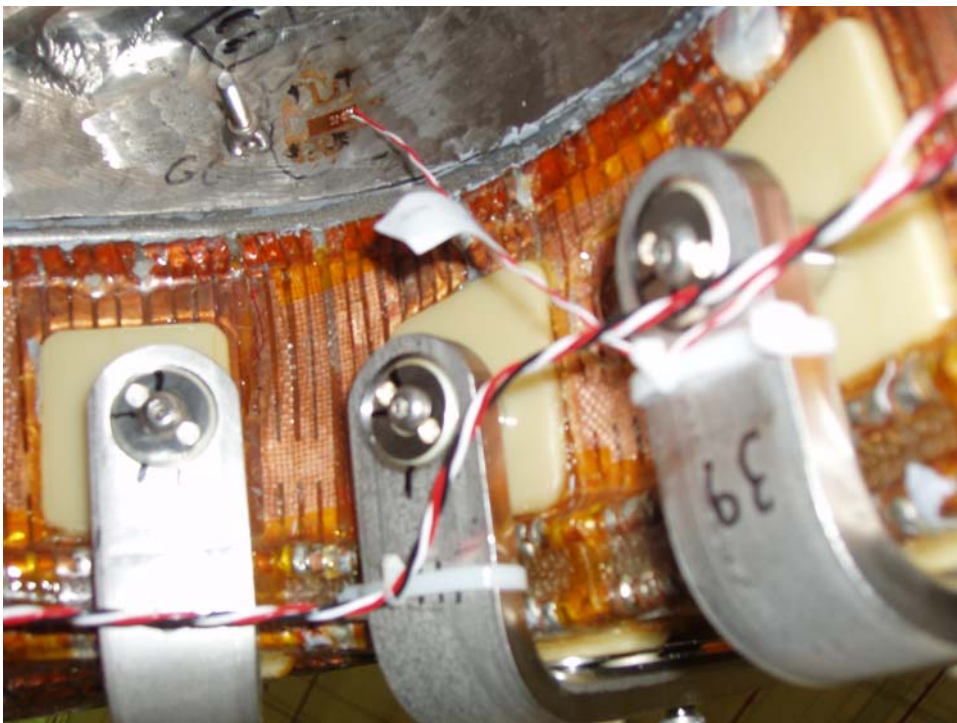
Figure 5-37 Strain gage at Clamp 42 - Side A

Figure 5-38 Strain gage (SG15) near lead block

Figure 5-39 Winding pack strain gage (dummy) at Clamp 7 - Side B
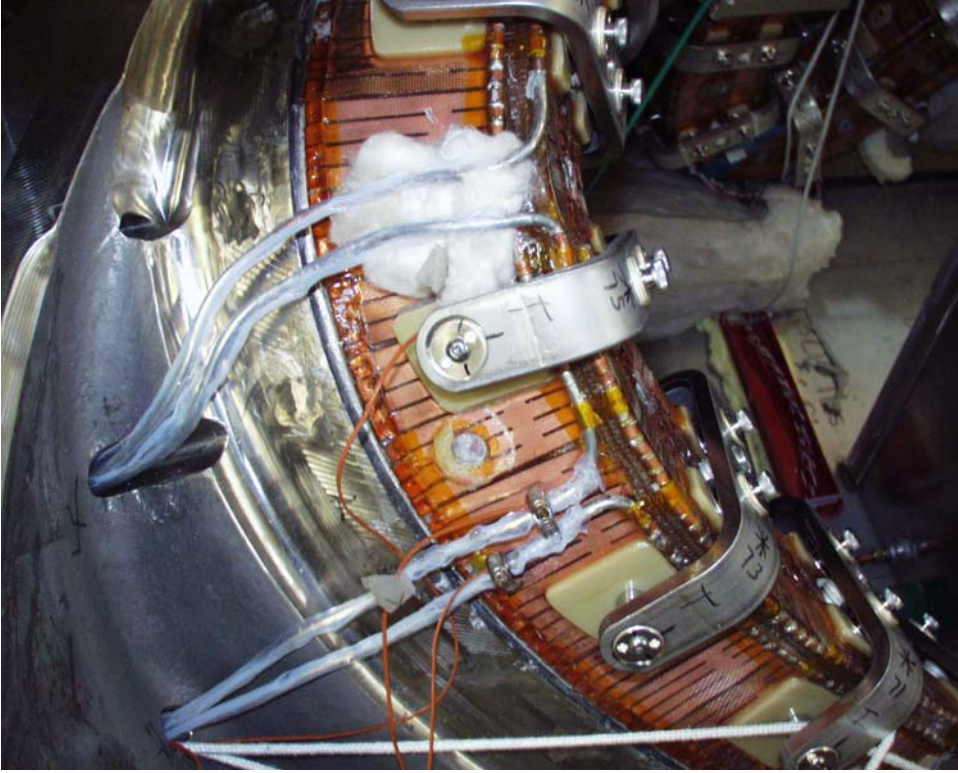
Figure 5-40 Winding pack thermocouple (TC17) under glass wool

5.4 Strain Gage Explorations[3]

---

15 Kamp Cold Test (121405)
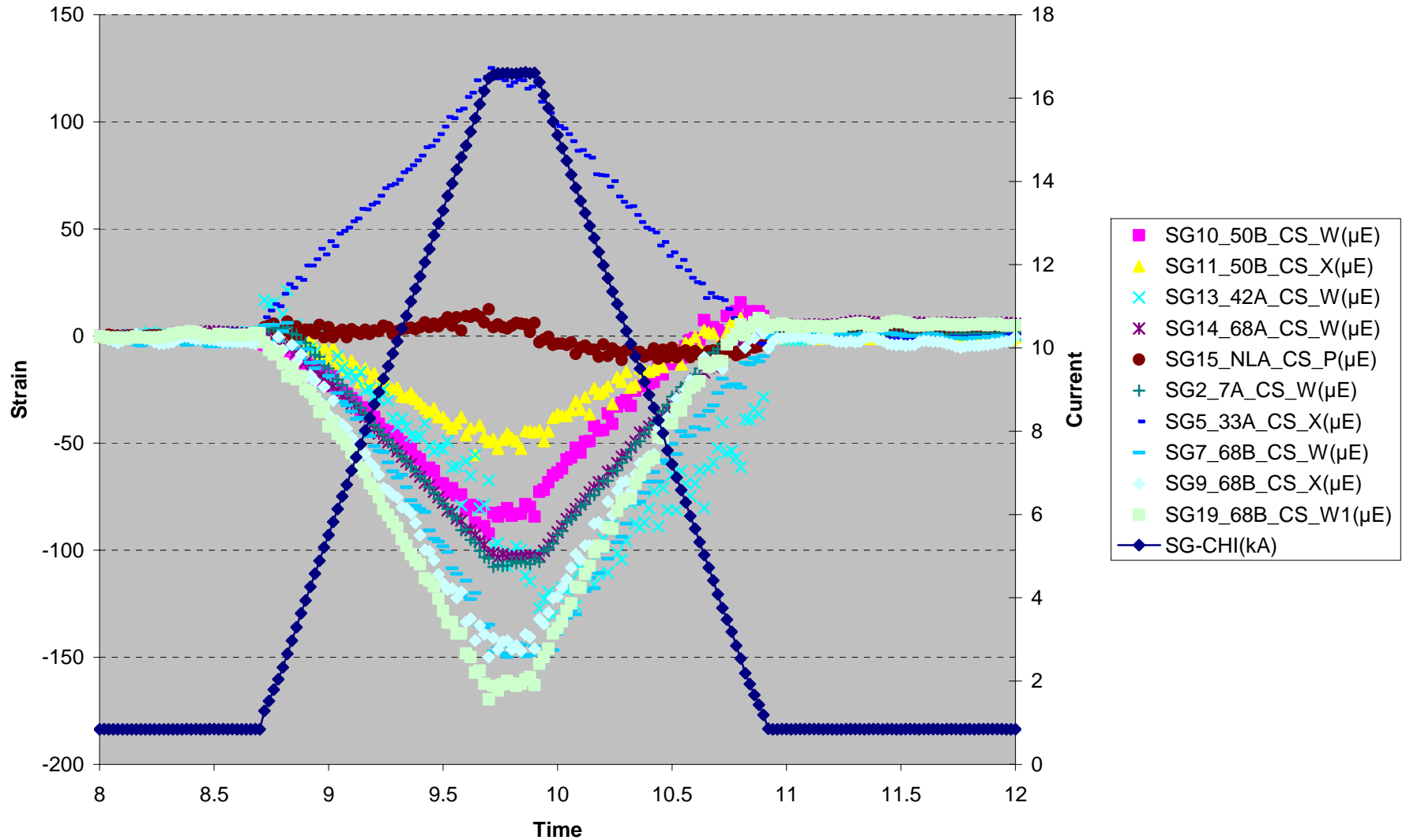
15 Kamp (warm test 121540)
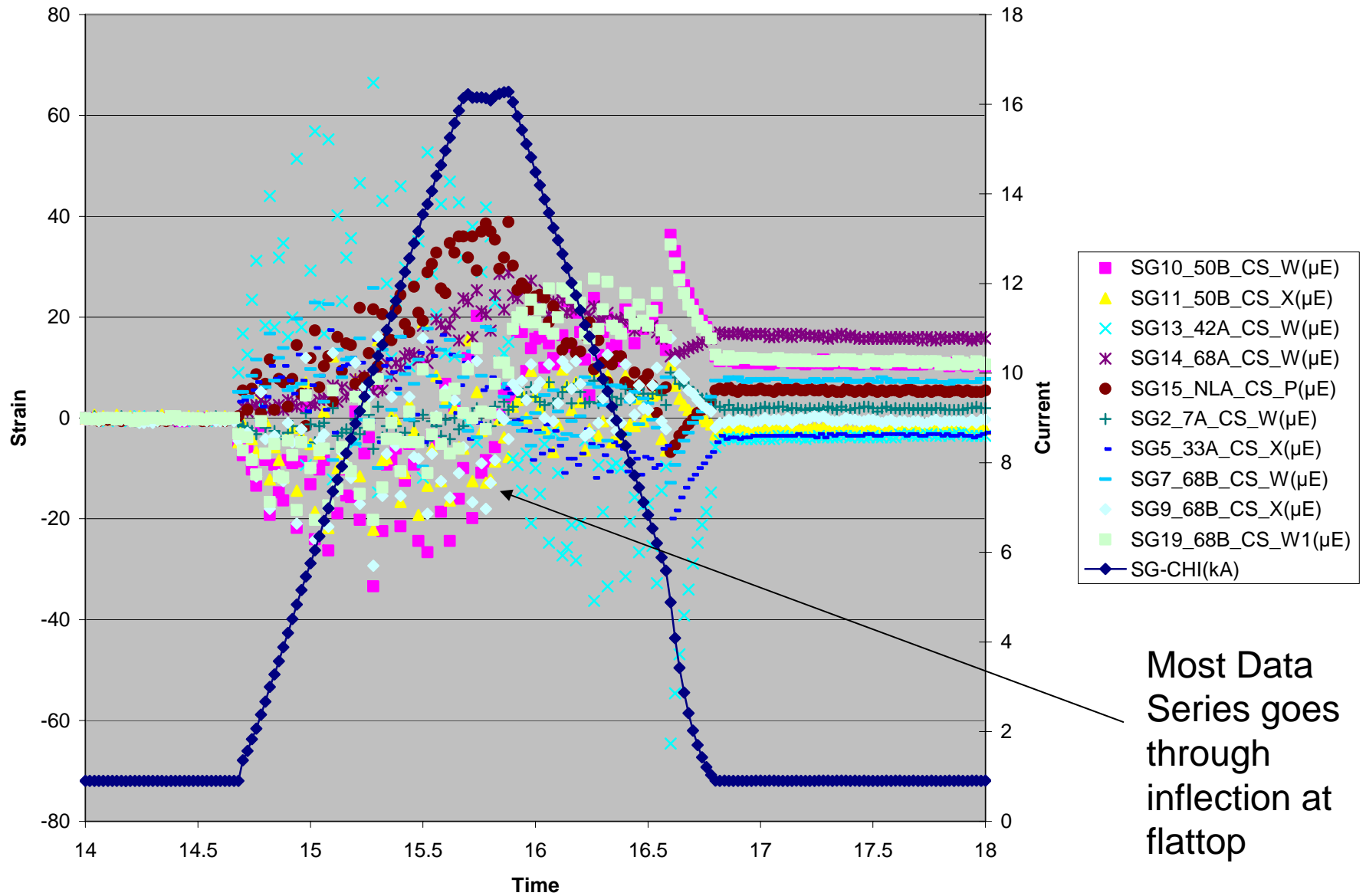
15 kamp (warm) Case after trip ?

Why would this occur? After the current waveform was terminated
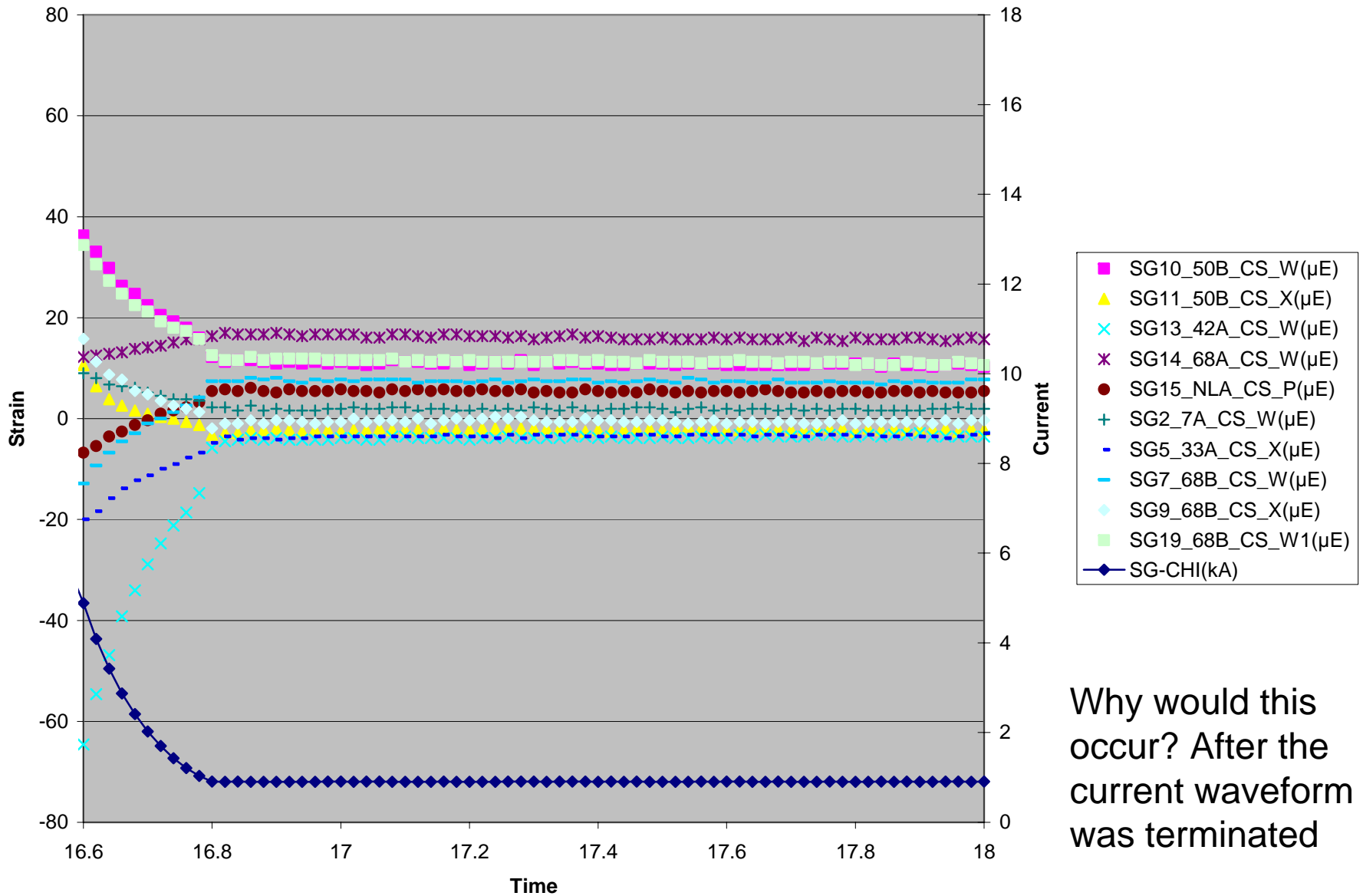
What about the other trips (35 Amp cold) 121412

Legend:
- SG10_50B_CS_W(µE)
- SG11_50B_CS_X(µE)
- SG13_42A_CS_W(µE)
- SG14_68A_CS_W(µE)
- SG15_NLA_CS_P(µE)
- SG2_7A_CS_W(µE)
- SG5_33A_CS_X(µE)
- SG7_68B_CS_W(µE)
- SG9_68B_CS_X(µE)
- SG19_68B_CS_W1(µE)
- SG-CHI(kA)

Gage Data appears to have expected shape after trip, jumps at trip may be vibratory
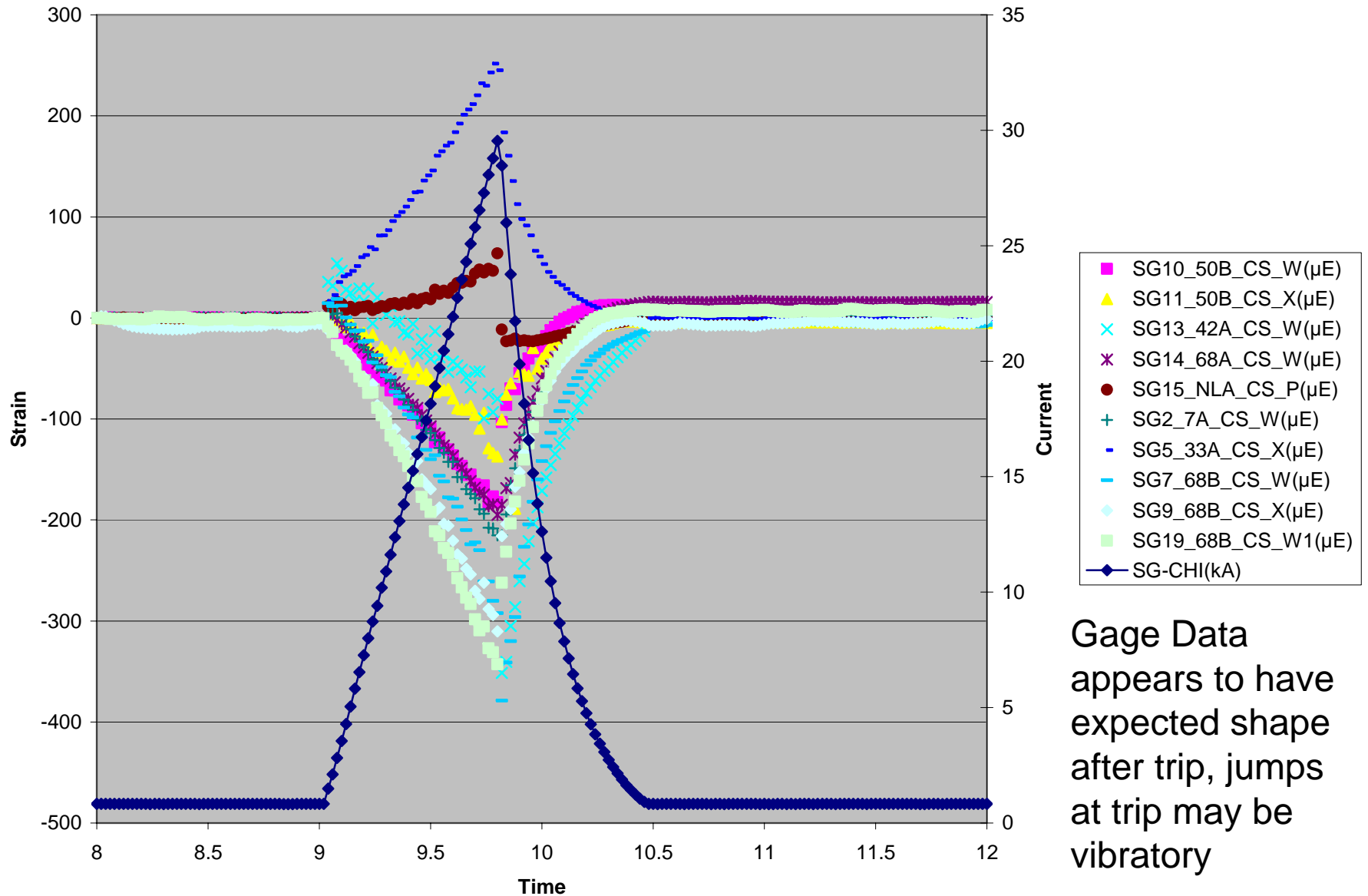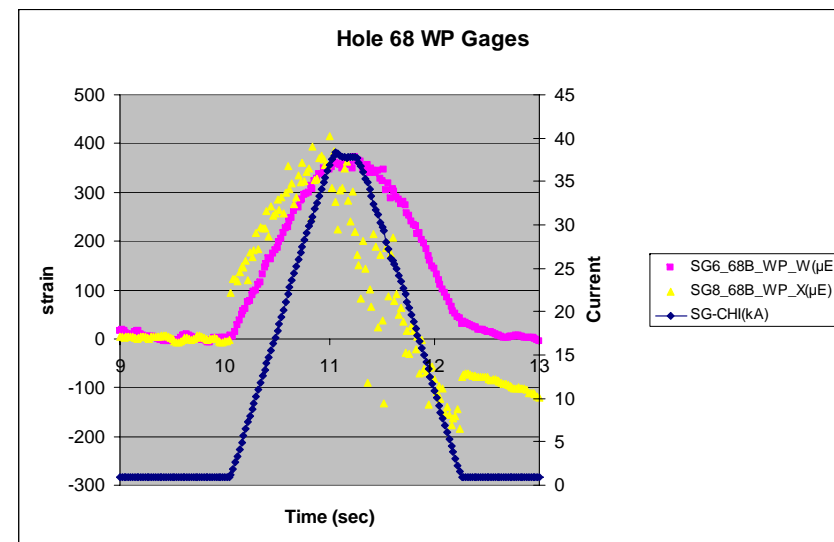
36.5 Kamp Case (121461)
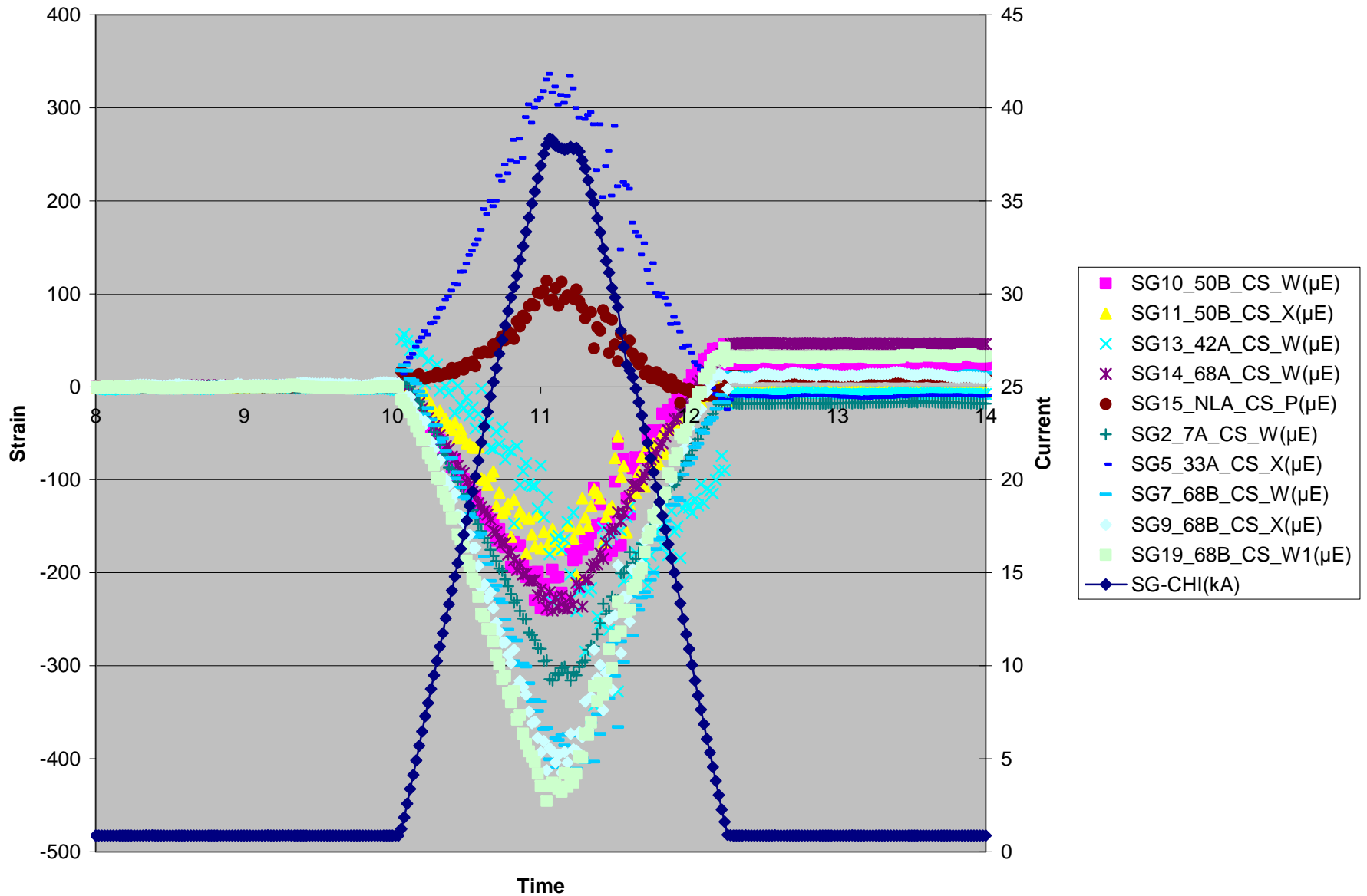
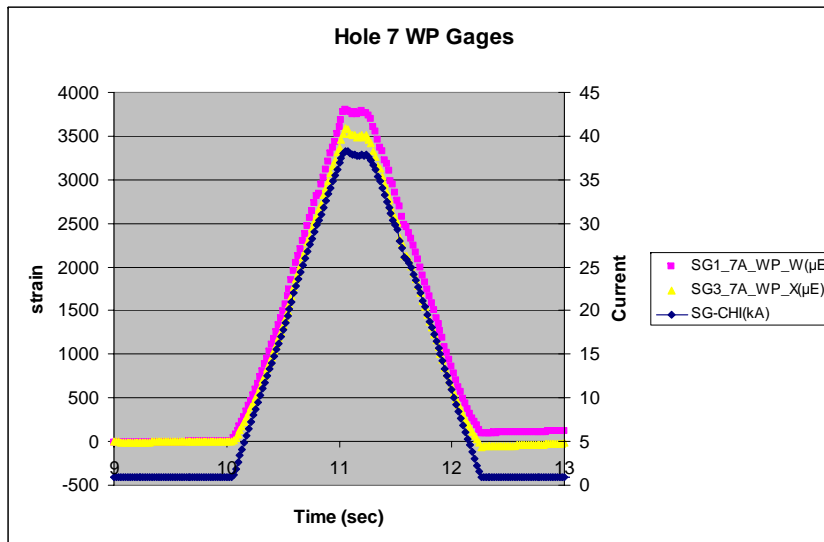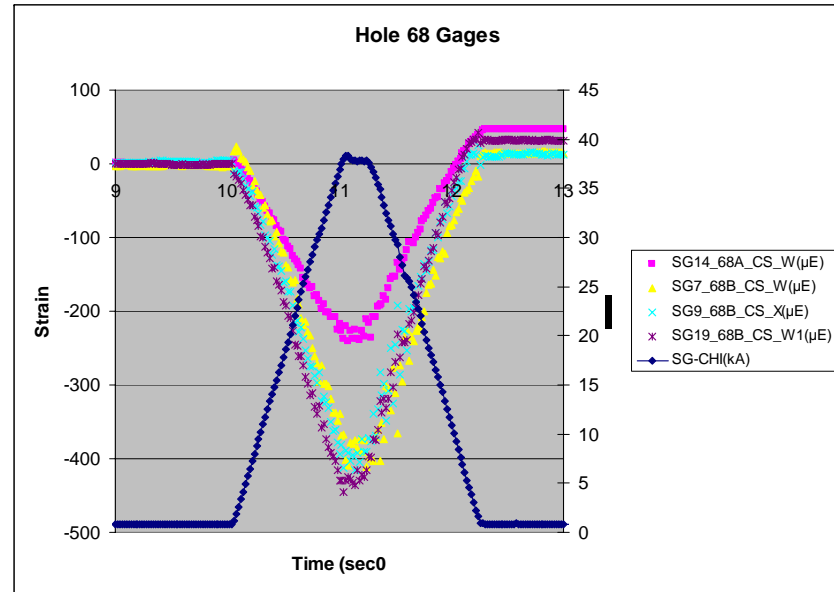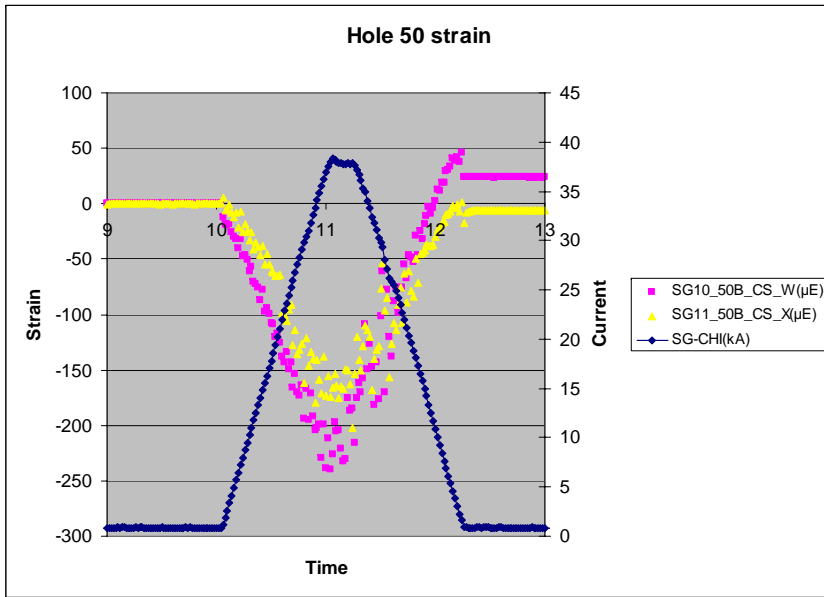# Winding Gage Plots

15 kamp Cold
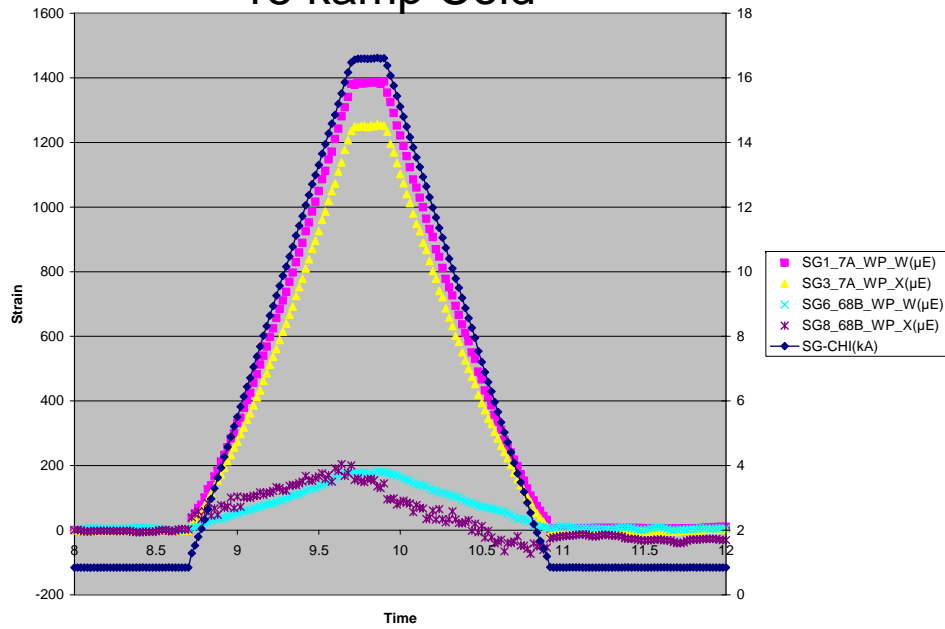
15 kamp Warm
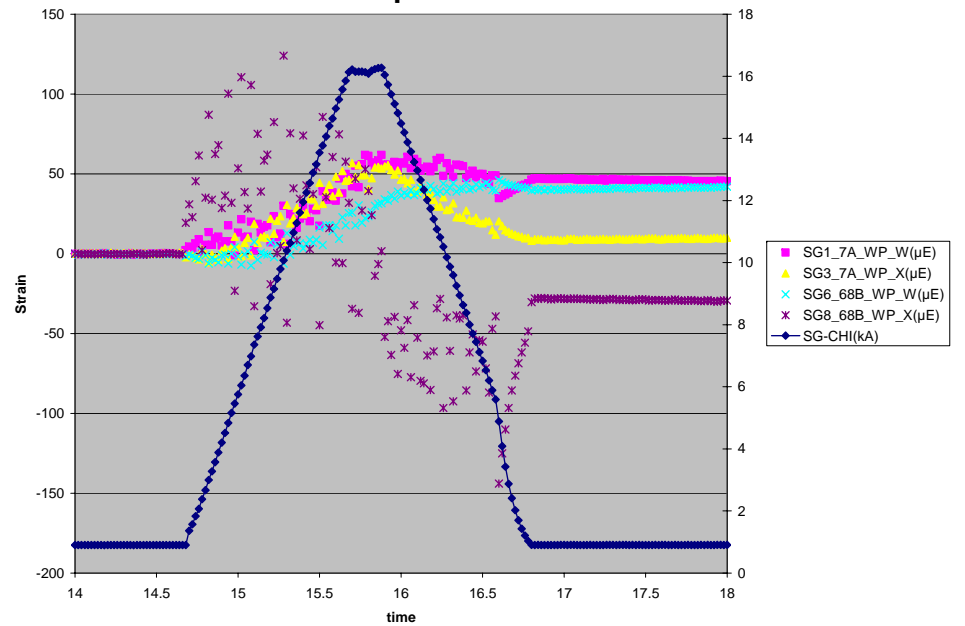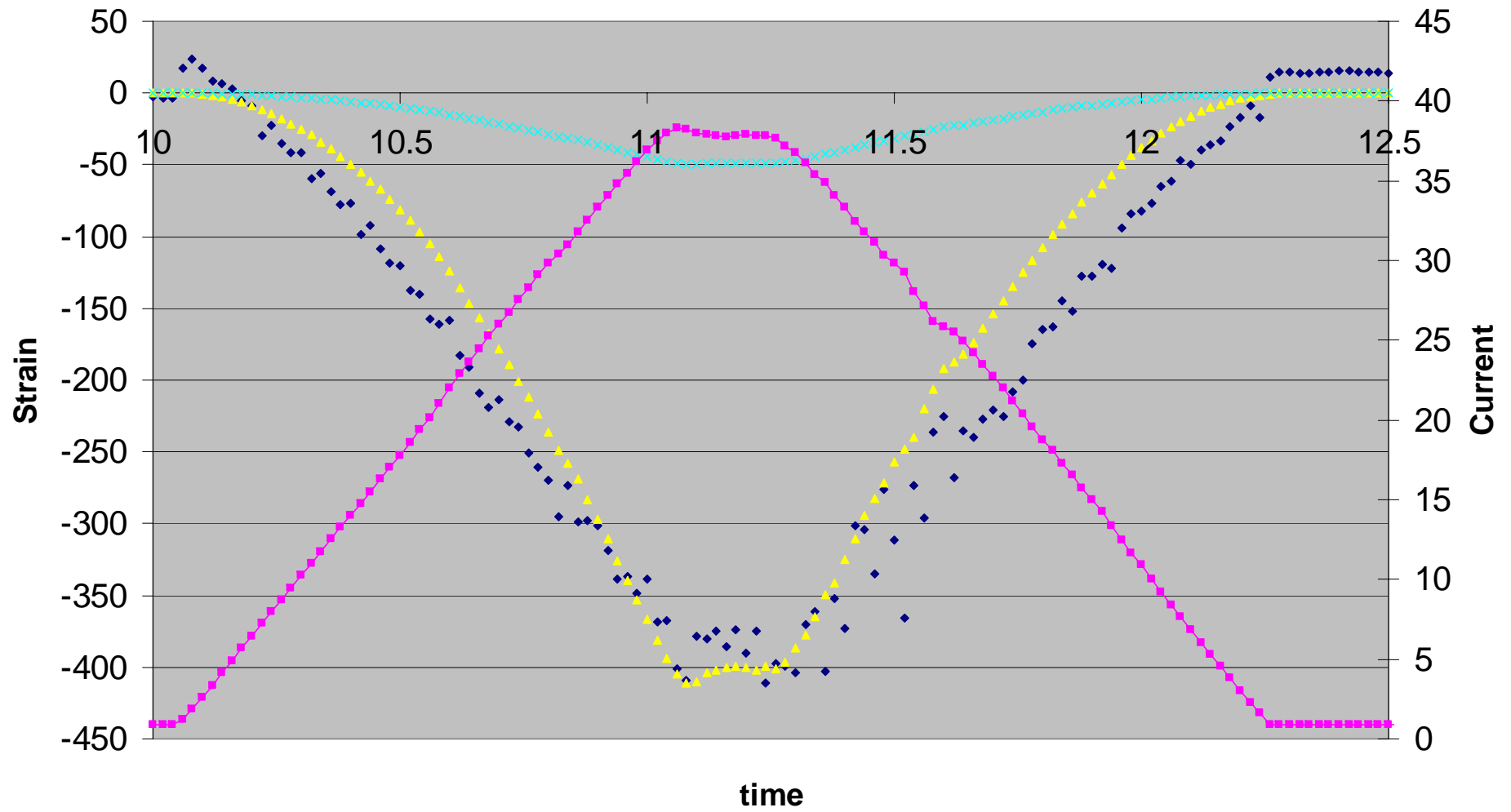
35 kamp Trip
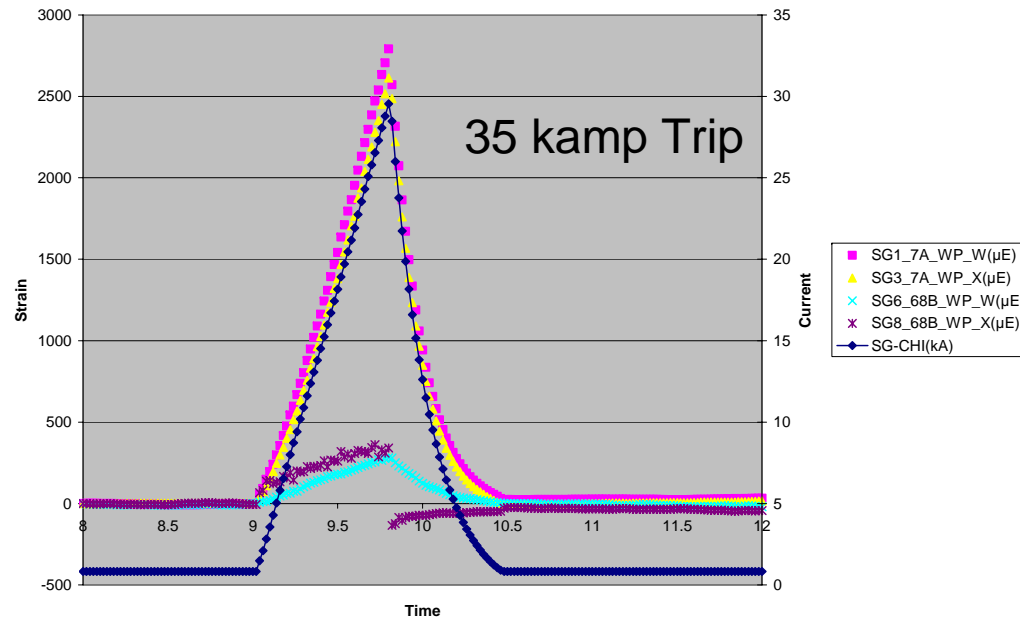
Hole strain comparison for shot 121461

Very Little chance that strain in two directions measured on like holes would be the same

36.4 Kamps, Gage 7, Hole 68, Side B, Winding Direction

Strain (left axis): 50, 0, -50, -100, -150, -200, -250, -300, -350, -400, -450

Current (right axis): 45, 40, 35, 30, 25, 20, 15, 10, 5, 0

time (x-axis): 10, 10.5, 11, 11.5, 12, 12.5

Legend: ♦ SG7_68B_CS_W(µE)   ▲ Predicted if peak value believed   × Ansys Predicted   ■ SG-CHI(kA)

Points

- Data does not match ANSYS in direction or magnitude except gage 15
- Strain readings in different directions at the same hole number give roughly the same delta strain.
- Turning the current off (Trip) seems to create a different strain profile for both cryogenic and room.
- Room data is all over the place and loosely follows a voltage profile for most gages.
- Cryogenic data is highly linear while the current is being controlled (voltage applied).
- Gage 15 away from the coils near the leads looks somewhat plausible even at room temperature. (Were its wires wrapped around the windings?)